Московский физико-технический институт (государственный университет)
Сколковский институт науки и технологий

ВЫПУСКНАЯ КВАЛИФИКАЦИОННАЯ РАБОТА
«Статистика краевого тока в двумерном топологическом изоляторе при наличии магнитной примеси»

(магистерская диссертация)

Студент: Курилович Павел Даниилович

Научный руководитель: Бурмистров Игорь Сергеевич, д. ф.-м. н.

Москва 2018

Moscow Institute of Physics and Technology (State University)
Skolkovo Institute of Science and Technology

MASTER'S THESIS
«Magnetic Impurity at the Edge of a Two-Dimensional Topological Insulator: the Full Counting Statistics of the Backscattering Current»

Student: Pavel Kurilovich

Thesis advisor: Igor Burmistrov, Ph.D., D.Sc.

Moscow 2018

Acknowledgements

First of all, I wish to express sincere gratitude to my thesis advisor Dr. Igor Burmistrov. Discussions with him were invaluable for my research and I learned a lot of advanced physical concepts and techniques from him.

I would also like to thank Vladislav Kurilovich, my twin brother and, at the same time, my co-worker. It was a pleasure to carry out research and discuss science with him. Several results of the present thesis were obtained in the joint effort with Vladislav.

Finally, I am grateful to Dr. Moshe Goldstein from Tel Aviv University and to Prof. Yuval Gefen from Weizmann Institute of Science. Conversations with them were of uttermost importance for my studies and helped me understand many aspects of non-equilibrium transport.

Contents

Chapter 1

Introduction

1.1 Topological insulators

Topological and geometric ideas often attracted the attention of physicists. Recently, the interest to topology was rekindled in the context of condensed matter physics by the discovery of topological insulators and topological superconductors [1], [2]. Topological insulators are novel materials and structures that insulate electric current in the bulk and, at the same time, host exotic conductive modes on their boundaries. The emergence of these modes results from the non-trivial topology of the electronic band structure in the bulk and is associated with strong spin-orbit coupling in the material. Boundary electronic states in topological insulators possess linear energy spectrum. The direction of movement of electrons in these states uniquely defines the direction of their spin. The latter feature is often referred to as spin-momentum locking.

Topological insulators might be realized in structures of different dimensionality. Two-dimensional topological insulators (2D TIs) and gapless edge states in them are in the main focus of the thesis. Still, it is worthwhile to briefly discuss three-dimensional topological insulators (3D TIs).

1.1.1 Three-dimensional topological insulators

Historically, the first materials found to be 3D TIs are $Bi_{1-x}Sb_x$ compounds. The existence of topological surface states in $Bi_{1-x}Sb_x$ was first predicted theoretically [3] and later confirmed experimentally [4]. Soon after that, a large number of other 3D TIs was discovered [5].

Surface states of a 3D TI have a Dirac-cone energy spectrum that spans the band gap of the bulk material. Due to spin-momentum locking of the surface states, their spin winds around the Dirac cone in the momentum space as depicted in Figure 1.1.

$TlBiSe_2$ is another example of a 3D TI. Conic energy dispersion of the surface states in this

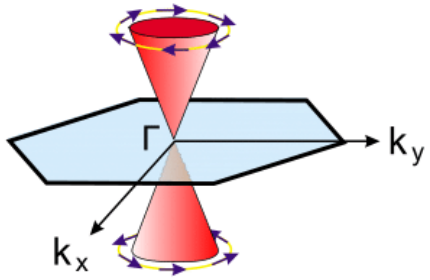

Figure 1.1: Schematic depiction of the Dirac-cone energy spectrum of the surface states in a three-dimensional topological insulator. The spin of the surface states wraps around the cone. The figure is adapted from [2].

topological insulator was measured by the means of angle-resolved photoemission spectroscopy [6]. We present the result of this measurement in Figure 1.2. Large bulk band gap of 0.35 eV makes $TlBiSe_2$ a promising material to probe topological properties at the room temperature.

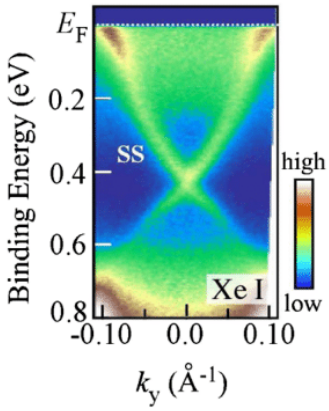

Figure 1.2: Result of angle-resolved photoemission spectroscopy measurement of surface state energy spectrum in $TlBiSe_2$ three-dimensional topological insulator. Dirac cone at the Γ-point can be easily recognized. Adapted from [6].

We note that because of time-reversal symmetry surface states come in pairs with the same energy but with the opposite momentums and spins. For this reason, conic point in the spectrum is protected against perturbations respecting time-reversal symmetry. If the time-reversal symmetry in the 3D TI is broken, then the gap in the spectrum might appear.

1.1.2 Two-dimensional topological insulators

In contrast to 3D TIs that host two-dimensional surface states, the main feature of 2D TIs is the presence of a pair of one-dimensional states localized near the edge of the structure. These edge states are counter-propagating and spin-momentum locked: electrons moving from left to right along the edge and electrons moving from right to left have their spins pointing in the opposite directions. For this reason, edge states in 2D TIs are often called helical. An important feature of 2D TIs is that the right moving edge states are linked via time-reversal symmetry to the left moving edge states. The spectrum of the edge electrons is linear and has Dirac point at $\boldsymbol{k} = 0$. Level crossing at the Dirac point is stable under perturbations respecting reversal symmetry. Typical spectrum of the edge states in a 2D TI is sketched in Figure 1.3.

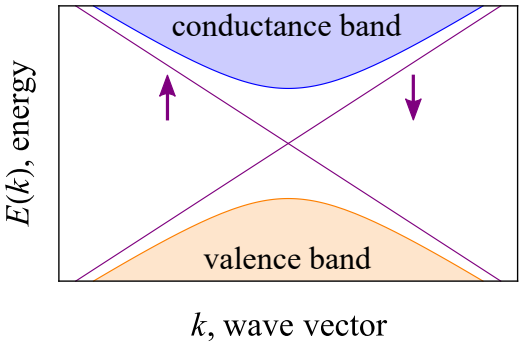

Figure 1.3: Schematic depiction of the energy spectrum of a 2D TI. Blue and orange parts of the spectrum correspond to conductance and valence bands in the bulk of the structure. Crossing purple lines correspond to one-dimensional edge states. Arrows denote the direction of spin of the edge states.

Time reversal symmetry protects the edge states from elastic backscattering on a potential disorder. In principle, this leads to the ideal ballistic charge conductance $G_0 = e^2/h$ along the helical edge ($2e^2/h$ for two parallel ideal edges). Moreover, the presence of edge states in a 2D TI gives rise to quantum spin Hall effect [7], [8].

Peculiar properties of the helical edge states and their insensitivity to potential disorder make 2D TIs great candidates for applications in different innovative fields of technology: from spintronics to quantum computing.

The first structure predicted to be a 2D TI is a narrow (001) CdTe/HgTe/CdTe quantum-well[1] with inverted order of bulk bands [9]. The existence of spin-momentum locked edge states in such heterostructures was demonstrated experimentally [10, 11, 12, 13, 14, 15, 16], confirming the theoretical predictions. Later, a multitude of other structures was found to be 2D TIs. Among them are InAs/GaSb quantum wells, WTe_2 monolayers, and Bi bilayers.

However, although ideal quantized ballistic conductance is observed for short samples with length ~ 1 μm, conductance is much smaller for long edges (see Figure 1.4 for a detailed example). This fact hints that the edge electrons move in a diffusive fashion on large scales. Moreover, the conductance saturates to a constant value at small temperatures.

The aforementioned experimental results required a theoretical explanation. In the non-interacting case, perturbations that respect time-reversal symmetry of the helical edge cannot induce backscattering. For instance, as it was mentioned, elastic backscattering from potential disorder is prohibited. However, the presence of inelastic processes [17] might drive conductance down from its ideal value. Moreover, localized magnetic moments near the helical edge might lead to backscattering of electrons [18, 19, 20, 21]. Electron-electron interactions might be also responsible for conductance reduction giving rise to many-particle backscattering processes [22] or to spontaneous breaking of time-reversal symmetry by the means of edge reconstruction [23]. The combined effect of electron-electron interactions and localized magnetic moments can further complicate the

[1] Generally speaking, to realize a two-dimensional topological insulator, $Cd_{1-x}Hg_xTe/HgTe/Cd_{1-x}Hg_xTe$ quantum wells with different orientations of growth might be used. In order to simplify the discussion and to shorten the text, we focus on the case of (001) quantum well with $x = 0$.

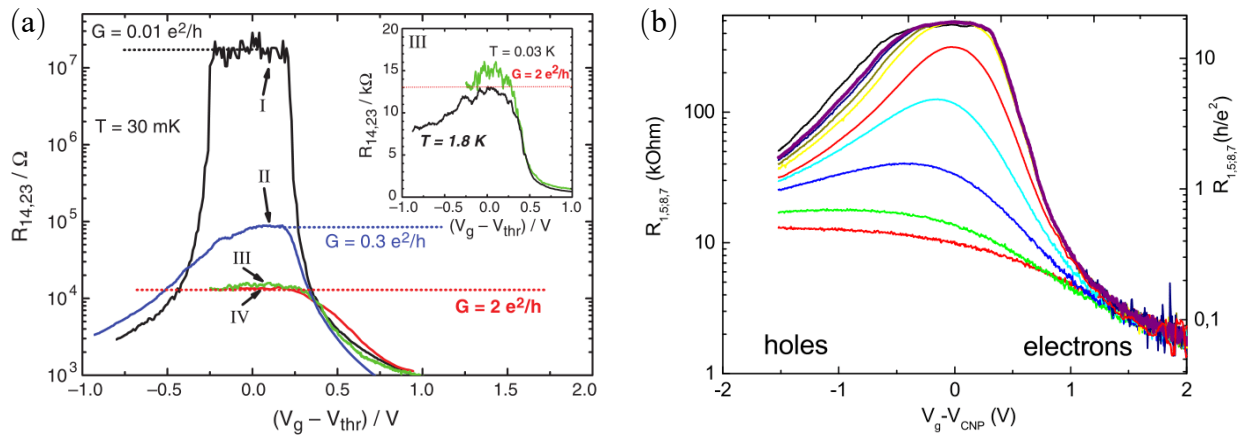

Figure 1.4: Resistance of Hall bar devices based on HgTe quantum wells as a function of gate voltage. (a) Devices (I), (II) have long edges (~ 10 μm), devices (III), (IV) have short edges (~ 1 μm). Adapted from [10]. (b) Device with a long edge (≈ 30 μm). Different curves correspond to T varying from 62 K to 1.5 K (bottom to top). Adapted from [15].

picture of the helical edge transport [24, 25, 26, 27, 28].

For 2D TIs based on CdTe/HgTe/CdTe and InAs/GaSb quantum wells, many aspects of experimental data might be explained qualitatively by suggesting that a large amount of charge puddles is formed near the helical edge [18]. Charge puddles might appear because the aforementioned semiconductor heterostructures have a narrow band gap in the bulk and, therefore, are very sensitive to fluctuations of the chemical potential induced by regular impurities. Whenever the chemical potential is shifted outside the gap, a small metallic region - a charge puddle - is generated.

Charge puddles located near the edge interact with the helical electrons differently depending on the parity of the number of electrons trapped inside the puddle. If this number is even, then the puddle serves as a source of inelastic scattering for the electrons. Contribution to the conductance from such puddles has a strong power-law temperature dependence, dying out quickly at small temperatures [17]. On the contrary, if the number of electrons in the puddle is odd, the situation is altered dramatically. In that case, the ground state of the puddle is doubly degenerate so that it effectively acts as a spin-1/2 magnetic impurity coupled to the helical electrons almost isotropically [18]. Puddles of the latter type account for the correction to conductance that weakly depends on temperature. Therefore, charge puddles with the odd number of electrons determine the transport of semiconductor heterostructures at small temperatures.

However, not only charge puddles might induce significant backscattering. Usual magnetic impurities might also be responsible for the suppression of ballistic conductance [19, 20, 21]. A typical example of such magnetic impurities are Mn^{2+} atoms with $S = 5/2$ built into the lattice of a CdTe/HgTe/CdTe quantum well.

One of the ways to distinguish between possible sources of electron backscattering in a 2D TI

is to investigate the noise of the current flowing through the edge. In a recent work [29], authors investigated the finite-frequency current noise induced by a single magnetic moment localized near the helical edge. Keeping in mind the charge puddle, they assumed that the magnetic moment has $S = 1/2$ and is coupled to the helical edge electrons in a weakly anisotropic way. Authors determined that the noise strongly depends on the frequency at scales much smaller than the temperature. Interestingly, they realized that electron backscattering might happen in pairs under certain conditions, i.e. the backscattering process might super-Poissonian.

1.2 Statement of the problem

In the present thesis, we consider a single magnetic impurity[2] with spin S weakly coupled to the helical edge of a 2D TI (see Figure 1.5 for clarification). We assume that voltage V is applied to the leads attached to the edge. In that case, the current flowing along the helical edge can be decomposed into two parts: positive ideal ballistic current I_0 and negative backscattering current ΔI. The latter part of the total current is studied in the manuscript.

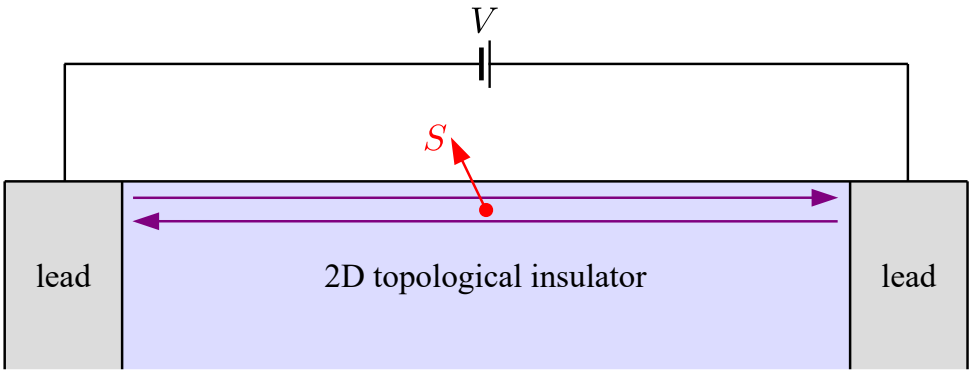

Figure 1.5: Sketch of the considered system. Purple arrows denote the helical edge states. Red arrow denotes the magnetic impurity. Voltage V is applied to the leads.

On the one hand, contrary to the work [29], we do not discuss finite frequency properties of the system, limiting ourselves to zero-frequencies. On the other hand, we do not assume that $S = 1/2$ and that the coupling between the impurity and electrons is weakly anisotropic. Moreover, whenever possible, we calculate higher cumulants of the backscattering current ΔI. In certain limits, we determine the full counting statistics of the backscattering current.

[2]Throughout the thesis we will mostly discuss magnetic impurities. However, our theory is rather general and might be applied to different types of magnetic moments localized near the edge of a 2D TI.

1.3 Outline of the thesis

In Chapter 2 we formulate the theoretical model of the considered system that is utilized throughout the thesis. We review Bernevig-Hughes-Zhang model of a 2D TI and discuss how it can be used to describe helical edge states. We present the Kondo-type Hamiltonian of the interaction between the edge states and the magnetic impurity.

In Chapter 3 we outline the general strategy for the calculation of cumulants of the backscattering current. The approach is based on the generalized master equation for the density matrix of the magnetic impurity. We discuss renormalizations that appear in the problem. The results of this chapter are partially published in [20].

In Chapter 4 we evaluate the average backscattering current for arbitrary spin S of the magnetic impurity. For $S = 1/2$ we present the expression for the variance of the number of backscattered electrons that is valid at arbitrary voltage. Moreover, we find the full counting statistics of the backscattering current in the large voltage regime for $S = 1/2$.

In Chapter 5 we discuss zero-frequency noise for arbitrary S at large voltages. We calculate the Fano factor of the backscattering current for different parameters of the electron-impurity coupling.

Chapter 2

Theoretical model

In this chapter, we outline the theoretical framework that forms the basis for the thesis. We formulate the general theoretical model that describes the behavior of electrons occupying the helical edge of a 2D TI and their interaction with a magnetic impurity. We begin by explaining the way in which the helical edge states appear in the clean case, i.e. when no magnetic impurities are present in the 2D TI. We briefly remind the reader of the Bernevig-Hughes-Zhang model [9] that is commonly used to describe the low-energy behavior of electrons in 2D TIs. Although in its initial formulation the model describes electrons in TIs based on (001) CdTe/HgTe/CdTe quantum wells, its general form happens to be universal. Therefore, after the proper redefinition of parameters, it can be utilized to describe edge states in different topological insulators. For this reason, without restriction of generality, in the thesis, we focus on the case of CdTe/HgTe/CdTe quantum well.

2.1 Bernevig-Hughes-Zhang model

Bernevig-Hughes-Zhang (BHZ) model describes the low-energy behaviour of non-interacting electrons confined within the 2D (001) CdTe/HgTe/CdTe quantum well. The single particle version of the corresponding Hamiltonian reads

$$H_{\text{BHZ}}(\boldsymbol{k}) = -Dk^2 I_{4\times 4} + \begin{pmatrix} h(\boldsymbol{k}) & 0 \\ 0 & h^\star(-\boldsymbol{k}) \end{pmatrix}, \quad h(\boldsymbol{k}) = \begin{pmatrix} M - Bk^2 & Ak_+ \\ Ak_- & -M + Bk^2 \end{pmatrix}, \tag{2.1}$$

where $I_{4\times 4}$ is a 4×4 unit matrix, $\boldsymbol{k} = (k_x, k_y)$, $k^2 = k_x^2 + k_y^2$, and $k_\pm = k_x \pm ik_y$. Hamiltonian (2.1) operates in the basis consisting of four states spatially quantized in z-direction, i.e. in the direction perpendicular to the plane of the 2D TI. These states are commonly denoted as $|E_1, +\rangle$, $|H_1, +\rangle$, $|E_1, -\rangle$, $|H_1, -\rangle$. They can be characterized by projection m_z of the angular momentum in z-

direction. Electronic states $|E_1, \pm\rangle$ have $m_z = \pm 1/2$ respectively while heavy hole states $|H_1, \pm\rangle$ have $m_z = \pm 3/2$. This implies that Hamiltonian (2.1) has strong inbuilt spin-orbit coupling. For instance, states with different m_z are mixed by finite k due to $Ak_\pm$ terms. Details of the "inner" structure of the basis states as well as the corresponding envelope functions can be found in [9, 30]. It is worthwhile to mention that BHZ model respects time-reversal symmetry, which is indicated by the connection of blocks of BHZ Hamiltonian. Moreover, BHZ Hamiltonian is rotationally invariant, i.e. it preserves its form under the rotation of axes x and y. The energy spectrum of the BHZ model is given by

$$E(k) = -Dk^2 \pm \sqrt{(M - Bk^2)^2 + A^2k^2}. \tag{2.2}$$

Energy bands have double spin degeneracy. Typically, $B < 0$, $D < 0$, and $|D| < |B|$ so that there is a gap of $2|M|$ in the spectrum. Therefore, the considered system is a 2D band insulator in the bulk. At $M > 0$ the conduction band primarily consists of states $|E_1, \pm\rangle$, while the valence band consists of states $|H_1, \pm\rangle$. If M is changed to be negative, the band inversion occurs and $|H_1, \pm\rangle$ states float above $|E_1, \pm\rangle$ states. As it will be discussed in the next section, band inversion corresponds to a topological phase transition accompanied with the appearance of two counter-propagating gapless spin-momentum locked edge states.

Physically, gap parameter M can be tuned by varying the thickness d of HgTe layer of the quantum well. In the case $d < 6.3$ nm the parameter $M > 0$, while for $d > 6.3$ nm $M < 0$. Realistic values of parameters of BHZ Hamiltonian are summarized in the Table 2.1. The energy spectrum of 2D bulk electrons in the CdTe/HgTe/CdTe quantum well with $d = 7$ nm is depicted in the Figure 2.1. As it was mentioned, the spectrum of BHZ model is rotationally invariant. For this reason, we present here only a single cut of the full two-dimensional spectrum. We note that the conduction band has a stronger dispersion than the valence band.

Finally, we underline that BHZ model is a two-band model and it is applicable only when all the other bands can be treated as a perturbation. This is typically the case for CdTe/HgTe/CdTe quantum wells with the width of HgTe layer ≈ 6.3 nm.

d, nm	A, eV · nm	B, eV · nm^2	D, eV · nm^2	M, eV
5.5	0.39	-0.48	-0.31	0.009
7.0	0.37	-0.69	-0.51	-0.010

Table 2.1: Realistic parameters of BHZ Hamiltonian (2.1). Parameters for two different quantum well thicknesses d are presented. Values are adapted from [1].

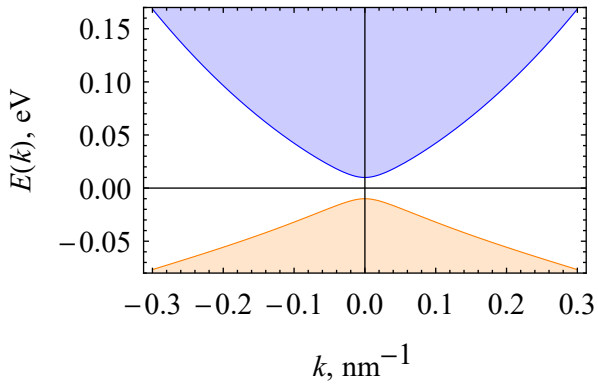

Figure 2.1: Cut of electronic energy spectrum $E(k)$ in BHZ model. Parameters from Table 2.1 for $d = 7$ nm are used.

2.2 Topological order and edge states

In this section we discuss the topological nature of band inversion in BHZ model and outline how it results in the appearance of the gapless helical edge states. The first step in revealing the topology behind BHZ Hamiltonian is to introduce the concept of Chern number.

2.2.1 Chern number

In order to define Chern number we recall that Hamiltonian 2.1 consists of two blocks connected via time-reversal symmetry. Symmetry relation between the blocks allows us to consider only the upper-left block. Part of this block that has a non-trivial spin structure is given by 2×2 hermitian matrix $h(\boldsymbol{k})$. It can be parametrized as

$$h(\boldsymbol{k}) = \boldsymbol{\sigma} \cdot \boldsymbol{d}(\boldsymbol{k}), \quad \boldsymbol{d}(\boldsymbol{k}) = (Ak_x, -Ak_y, M - Bk^2), \quad \boldsymbol{\sigma} = (\sigma_x, \sigma_y, \sigma_z). \tag{2.3}$$

Here σ_x, σ_y, and σ_z are Pauli matrices acting in $|E_1, +\rangle$, $|H_1, +\rangle$ subspace. We introduce the normalized version of the vector $\boldsymbol{d}(\boldsymbol{k})$: $\boldsymbol{n}(\boldsymbol{k}) = \boldsymbol{d}(\boldsymbol{k})/|\boldsymbol{d}(\boldsymbol{k})|$. Non-trivial topology manifests itself in a finite value of the number

$$W = \frac{1}{4\pi} \int dk_x dk_y \, \boldsymbol{n}(\boldsymbol{k}) \cdot \left[\frac{\partial \boldsymbol{n}(\boldsymbol{k})}{\partial k_x} \times \frac{\partial \boldsymbol{n}(\boldsymbol{k})}{\partial k_y} \right]. \tag{2.4}$$

Integer quantity W is called Chern number, it describes the number of times the vector $\boldsymbol{n}(\boldsymbol{k})$ wraps around the three-dimensional sphere. In other words, Chern number is the winding number for the vector field $\boldsymbol{n}(\boldsymbol{k})$. We note that $W = 0$ whenever M and B have a different sign. This happens because in that case the sign of $n_z(\boldsymbol{k}) \propto M - Bk^2$ is either always negative or always positive. We assume that $B < 0$ which means that the winding number nullifies for $M > 0$. Therefore, the direct order of energy bands of the quantum well corresponds to the trivial topology of the insulator. However, for $M < 0$ the sign of n_z changes at $k = \sqrt{M/B}$, giving rise to the winding number

$W = 1$. This implies that band inversion puts the insulator into a topologically non-trivial state. We will discuss the consequences of this non-trivial topology in the next subsection.

2.2.2 Edge states in Bernevig-Hughes-Zhang model

According to the general statement, known as bulk-boundary correspondence, gapless edge states always appear on the boundary between two media with different winding numbers [1], [2]. For systems characterized by 2×2 Hamiltonians of the form $h(\boldsymbol{k})$, the number of edge states is given by the difference of winding numbers. In the case of BHZ model, the number of edge modes is doubled because the total Hamiltonian consists of two blocks linked via time-reversal symmetry. Therefore, a pair of edge states connected by time-reversal symmetry appear whenever a topologically non-trivial BHZ-type insulator ($W = 1$) is put in contact with a trivial insulator or vacuum ($W = 0$).

We proceed by analytically investigating the structure of the edge states in BHZ model. For the sake of simplicity, we assume that a semi-plane of topologically non-trivial BHZ insulator is restricted by vacuum which is modeled by zero boundary conditions for the electron wave function. We assume that vacuum spans the whole of $x > 0$ semi-plane. In that case one needs to solve the following Schrödinger equation:

$$H^{ij}_{\text{BHZ}}(-i\partial_x, k_y)\psi_j(x, k_y) = E\psi_i(x, k_y), \quad \psi_i(x = 0, k_y) = 0, \quad i = 1, ..., 4. \tag{2.5}$$

We note that due to the block structure of Hamiltonian (2.1) all solutions can be associated either with the upper block or with the lower block. For any solution $\psi^{\uparrow}_i(x, k_y)$ associated with the upper block $\psi^{\uparrow}_i(x, k_y) \equiv 0$, $i = 3, 4$, while for any solution $\psi^{\downarrow}_i(x, k_y)$ associated with the lower block $\psi^{\downarrow}_i(x, k_y) \equiv 0$, $i = 1, 2$. Due to the time-reversal symmetry, solutions in the upper block that have energy E and wave vector k_y generate solutions with the same energy E and wave vector $-k_y$ in the lower block according to the following rule: $\psi^{\downarrow}_i(x, -k_y) = (\psi^{\uparrow}_{i-2}(x, k_y))^{\star}$, $i = 3, 4$. Therefore, to gather the full information about the eigenstates of the system it is enough to work with the upper block of BHZ Hamiltonian. Schrödinger equation restricted to the upper block reads

$$\begin{pmatrix} M - (B + D)(-\partial^2_x + k^2_y) & A(-i\partial_x + ik_y) \\ A(-i\partial_x - ik_y) & -M + (B - D)(-\partial^2_x + k^2_y) \end{pmatrix} \begin{pmatrix} \psi^{\uparrow}_1 \\ \psi^{\uparrow}_2 \end{pmatrix} = E \begin{pmatrix} \psi^{\uparrow}_1 \\ \psi^{\uparrow}_2 \end{pmatrix}, \tag{2.6}$$

where $\psi^{\uparrow}_{1/2}(x = 0) = 0$. Our goal is to find the solution of equation (2.6) localized near the edge of the system and to show that it is indeed present when M and B are of the same sign. In principle, it is possible to cope with this task for any values of parameters of the system. However, for

illustrative purposes and in order to avoid bulky derivations we restrict ourselves to the electron-hole symmetric case $D = 0$. We start with considering a zero wave vector $k_y = 0$. Then the solution to (2.6) is given by a superposition of exponents $e^{\lambda x}$, where λ satisfies the following secular equation:

$$B^2\lambda^4 - (A^2 - 2BM)\lambda^2 + M^2 - E^2 = 0. \tag{2.7}$$

As long as we are interested in localized solutions, we assume that two roots of equation (2.7) have a positive real part and two roots have a negative real part. Roots with a negative real part are non-physical as they correspond to solutions exponentially growing into the bulk. Therefore, we stick to two roots with a positive real part and call them λ_- and λ_+. In that case it is trivial that $\psi^{\uparrow}_{1/2} = C_{1/2}(e^{\lambda_- x} - e^{\lambda_+ x})$ to satisfy the boundary conditions. On the other hand (2.6) implies

$$(M - E)\int_{-\infty}^{0} dx\psi^{\uparrow}_1(x) + B\partial_x\psi^{\uparrow}_1(0) = 0, \quad (M + E)\int_{-\infty}^{0} dx\psi^{\uparrow}_2(x) + B\partial_x\psi^{\uparrow}_2(0) = 0. \tag{2.8}$$

Combining these equations, we find that $B\lambda_-\lambda_+ = M \pm E$ so that $E = 0$. Moreover, we see that two roots of (2.7) with a positive real part exist only when M and B have the same sign, i.e. when the topological winding number W equals to unity. In that case we find (assuming $A > 0$)

$$\lambda_\pm = \frac{A}{2|B|}\left(1 \pm \sqrt{1 - \frac{4BM}{A^2}}\right) \tag{2.9}$$

and up to normalization the solution at $k_y = 0$ is given by

$$\begin{pmatrix}\psi^{\uparrow}_1\\ \psi^{\uparrow}_2\end{pmatrix} = \theta(-x)(e^{\lambda_- x} - e^{\lambda_+ x})\begin{pmatrix}1\\ i\end{pmatrix}, \qquad \psi^{\uparrow}_{3/4} = 0. \tag{2.10}$$

In the realistic case $4BM \ll A^2$ the length scale $\lambda_+ \approx A/|B|$ and $\lambda_- \approx |M|/A$. This implies $\lambda_- \ll \lambda_+$ so that the penetration depth of the edge state is $1/\lambda_-$. For the parameters of BHZ model presented in Table 2.1 we find $1/\lambda_+ \sim 1$ nm and $1/\lambda_- \sim 40$ nm. We see that $1/\lambda_+$ is of the atomic scale. Therefore, for such choice of parameters, the analysis for $|x| \lesssim 1/\lambda_+$ is, strictly speaking, invalid. However, on the large scales, we can neglect the quickly decaying exponent and safely use the obtained result. Treating finite k_y as a perturbation, we find that to the lowest order in k_y the energy dispersion of the discussed state is

$$E_{\uparrow}(k_y) = -Ak_y. \tag{2.11}$$

The time reversed solution of equation (2.6) is

$$\begin{pmatrix} \psi_3^{\downarrow} \\ \psi_4^{\downarrow} \end{pmatrix} = \theta(-x)(e^{\lambda_- x} - e^{\lambda_+ x}) \begin{pmatrix} 1 \\ -i \end{pmatrix}, \qquad \psi_{1/2}^{\downarrow} = 0. \tag{2.12}$$

Perturbative energy dispersion for this solution is

$$E_{\downarrow}(k_y) = Ak_y. \tag{2.13}$$

It is possible to verify that the dispersion relations (2.11) and (2.13) are exact for BHZ model with $D = 0$ [31]. Finite D alters the dispersion relations as

$$E_{\uparrow/\downarrow}(k_y) = -\frac{D}{B}M \mp A\sqrt{\frac{B^2 - D^2}{B^2}}k_y \tag{2.14}$$

Finishing this section, we mention that it is possible to describe the edge states of a 2D TI with the effective 2×2 Hamiltonian operating in the edge state subspace:

$$H_0(k_y) = -vk_y\sigma_z. \tag{2.15}$$

In this expression we omitted possible constant energy shifts, the velocity v is determined by (2.14), and σ_z is a Pauli matrix acting in the edge state subspace. We note that although it is temping to think that $\boldsymbol{\sigma}/2$ corresponds to the spin of the edge states, this is, strictly speaking, not the case. Indeed, according to (2.10) and (2.12) each edge state is a superposition of states with $m_z = \pm 1/2$ and $m_z = \pm 3/2$. Therefore, the edge states are not spin polarized. Still, the edge electrons moving in one direction have their average angular momentum pointing up, while electrons moving in the other direction have their average angular momentum pointing down. For this reason we will often refer to $\boldsymbol{s} = \boldsymbol{\sigma}/2$ as the spin of the edge electrons, keeping in mind the subtleties behind such notation.

Obtained edge states are robust to perturbations preserving the time-reversal symmetry of the electron system. As a consequence, they are protected from elastic backscattering on a potential disorder. However, magnetic impurities can induce electron backscattering and perturb the ideal conductivity of the helical edge of a 2D TI.

2.3 Magnetic impurity in Bernevig-Hughes-Zhang model

In this section, we discuss the way in which a magnetic impurity can be treated within two-band BHZ approach discussed previously. Physical configuration we keep in mind is a sole Mn^{2+} atom with spin $S = 5/2$ built into the lattice of CdTe/HgTe/CdTe quantum well. The impurity atom might be located inside HgTe layer as well as in one of CdTe layers. We assume that the impurity is point-like for all relevant applications. However, for the validity of the subsequent derivations, the impurity still has to be large on the atomic scales. Due to the large dielectric constants and small effective masses of 3D HgTe and CdTe, this is the case. The Hamiltonian of the electron-impurity exchange interaction in the bulk of the 2D TI can be written as [19, 32]

$$H_{\mathrm{e-i}}^{\mathrm{2D}} = \delta(\boldsymbol{r} - \boldsymbol{r}_0) \begin{pmatrix} J_1 S_z & -iJ_0 S_+ & J_m S_- & 0 \\ iJ_0 S_- & J_2 S_z & 0 & 0 \\ J_m S_+ & 0 & -J_1 S_z & -iJ_0 S_- \\ 0 & 0 & iJ_0 S_+ & -J_2 S_z \end{pmatrix}, \tag{2.16}$$

where $\boldsymbol{r} = (x, y)$ and $\boldsymbol{r}_0 = (x_0, y_0)$ denotes the position of the impurity. Coupling constants J_1, J_2, J_0, and J_m can be expressed via 3D bulk electron-impurity coupling constants of HgTe and CdTe and via the z-dependant envelope functions of states $|E_1, \pm\rangle$ and $|H_1, \pm\rangle$ [19, 32].

We note that the Hamiltonian (2.16) preserves the total m_z projection of the whole system (electron and impurity) as well as the overall time-reversal symmetry. Despite this, the magnetic impurity breaks the time-reversal symmetry of the helical edge considered as a separate system.

In order to obtain the effective Hamiltonian of the interaction between the edge states and the magnetic impurity we project (2.16) onto the edge states subspace. This results in the following Hamiltonian [19, 20]:

$$H_{\mathrm{e-i}} = \delta(y - y_0) \frac{1}{\xi} \left| e^{\lambda_- x_0} - e^{\lambda_+ x_0} \right|^2 J_{ij} S_i \sigma_j. \tag{2.17}$$

Here ξ is the normalization constant defined by the condition $\xi = 2\int_{-\infty}^{0} dx \left| e^{\lambda_- x} - e^{\lambda_+ x} \right|^2$ and the coupling matrix is given by

$$J_{ij} = \begin{pmatrix} J_m & 0 & 2J_0 \\ 0 & J_m & 0 \\ 0 & 0 & J_z \end{pmatrix}, \qquad J_z = J_1 + J_2. \tag{2.18}$$

As a next step, in order to clarify the physics of the electron-impurity interaction Hamiltonian

(2.17), we consider scattering of a single helical edge electron with a given σ_z on the magnetic impurity. In this regard, it is convenient to introduce the effective spin $\boldsymbol{M}$ of the electron-impurity system, which is given by sum of the impurity spin $\boldsymbol{S}$ and $\boldsymbol{s} = \boldsymbol{\sigma}/2$ of the electron.

Hamiltonian (2.17) can be split into several contributions. The first contribution is $\propto J_z S_z s_z$. It is incapable of flipping the electron spin and the spin of the magnetic impurity and is, therefore, of little interest. The second contribution is $\propto J_m(S_- s_+ + S_+ s_-)$, where $s_\pm = s_x \pm i s_y$ and $S_\pm = S_x \pm i S_y$. It is responsible for processes in which the electron flies towards the impurity, both impurity and electron flip their spins, and the electron flies back. Such process is schematically depicted in Figure 2.2 (a). As a result, total $M_z = S_z + s_z$ is conserved. Albeit the discussed angular-momentum-conserving processes can backscatter single electrons, in the following chapters it will be shown that they cannot induce a persistent backscattering current ΔI. Finally, in Hamiltonian (2.17) there is a contribution $\propto J_0(S_+ + S_-)s_z$ that is responsible for processes in which the spin of the electron is not flipped but the impurity spin is flipped (see Figure 2.2 (b) for clarification). These processes do not preserve M_z and, combined together with $S_- s_+ + S_+ s_-$ processes, they induce the backscattering current.

At the first glance, the presence of terms that do not conserve z-projection of the angular momentum in Hamiltonian (2.17) might seem somewhat unexpected. However, they are completely justified physically because:

- The system in question has strong spin-orbit coupling.
- The system is not rotationally invariant.
- The edge state with the given $s_z = \pm 1/2$ actually corresponds to the superposition of states with the projection of the angular momentum $\pm 3/2$ and $\pm 1/2$.

Finishing this section, we introduce the dimensionless coupling matrix $\mathcal{J}$:

$$H_{\text{e-i}} = \frac{1}{\nu}\delta(y - y_0)\mathcal{J}_{ij} S_i s_j, \quad \mathcal{J}_{ij} = \frac{2\nu}{\xi}\left|e^{\lambda_- x_0} - e^{\lambda_+ x_0}\right|^2 J_{ij}, \quad s_j = \sigma_j/2. \tag{2.19}$$

Here $\nu = 1/2\pi v$ is the density of the edge states (per spin projection). Through the thesis we will assume that the dimensionless coupling constants $\mathcal{J}_{ij}$ are small, i.e. $|\mathcal{J}_{ij}| \ll 1$. This will allow for the perturbative treatment of the problem.

Figure 2.2: Different scattering processes of the helical edge electron (purple) on the magnetic impurity with $S = 1/2$ (red). Pale arrows denote the initial configuration while bright colors denote the final configuration. (a) Process induced by the J_m term, total M_z is conserved. (b) Process induced by J_0 term in the Hamiltonian, total M_z changes by unity.

2.4 Final formulation of the model

2.4.1 Inversion asymmetry of the quantum well

Before formulating the final version of the model used throughout the thesis, we discuss how inversion asymmetry of the quantum well may alter the picture of the edge states described in section 2.2. In the previous considerations, effects of the inversion asymmetry were neglected. However, for realistic CdTe/HgTe/CdTe quantum wells, inversion asymmetry might be of a great importance. We follow articles [32, 33, 34] in the discussion.

The overall inversion asymmetry of a CdTe/HgTe/CdTe quantum well comes from two main sources. First of all, both HgTe and CdTe have zinc blende structure and belong to tetrahedron symmetry group T_d which lacks inversion symmetry. Secondly, the presence of CdTe/HgTe interfaces further breaks the inversion symmetry of the system with the respect to the middle of the quantum well. Indeed, each interface has a corrugated atomic structure and there is a relative rotation of $\pi/2$ between the corrugations of the different interfaces. Results of [33] based on atomistic numerical calculations indicate that the interface inversion asymmetry is much more important than the bulk inversion asymmetry for narrow quantum wells with $d \approx d_c = 6.3$ nm. Therefore, in the present discussion, we mainly keep in mind the interface mechanism of the inversion symmetry breaking.

In terms of BHZ Hamiltonian, the presence of interface inversion asymmetry results in the appearance of the off-diagonal terms:

$$H_{\text{BHZ}} + H_{\text{IIA}} = -Dk^2 I_{4\times 4} + \begin{pmatrix} h(\boldsymbol{k}) & i\sigma_y\gamma \\ -i\sigma_y\gamma^\star & h^\star(-\boldsymbol{k}) \end{pmatrix}. \tag{2.20}$$

Parameter $|\gamma|$ defines the characteristic energy scale of interface inversion asymmetry. According to the atomistic calculations [33], $|\gamma = 5 - 10|$ meV for narrow CdTe/HgTe/CdTe quantum wells. Notice that finite value of γ breaks the rotational symmetry of BHZ Hamiltonian: after the

rotation of coordinate axes by angle θ in (x, y) plane $\gamma \to \gamma e^{2i\theta}$. Nevertheless, rotations by π still preserve the form of the Hamiltonian. This is consistent with the picture of corrugated interfaces. Moreover, the low-energy spectrum of the asymmetric quantum well remains rotationally invariant. γ manifests itself in breaking the spin degeneracy at $k \neq 0$:

$$E(k) = -Dk^2 \pm \sqrt{(A|k| \pm |\gamma|)^2 + (M - Bk^2)^2}. \tag{2.21}$$

Splitting of the electronic spectrum of the quantum well was recently experimentally detected [35]. Spectrum for the quantum well with $d = 7$ nm (see Table 2.1) and $|\gamma| = 5$ meV is depicted in Figure 2.3.

Inversion asymmetry does not break time-reversal symmetry, i.e. H_{IIA} term in the Hamiltonian (2.20) commutes with the time-reversal symmetry operator $\mathcal{T}$. For this reason, even large γ cannot destroy the edge states or open the gap in their spectrum when M and B are of the same sign. However, finite γ alters the energy dispersion of the edge states by renormalizing the velocity v in (2.15). In the electron-hole symmetric case $D = 0$ the dispersion relation is given by [34]

$$E_{\uparrow/\downarrow}(k_y) = \mp A \frac{|M|}{\sqrt{M^2 + |\gamma|^2}} k_y \tag{2.22}$$

which is to be compared with (2.11) and (2.13). Moreover, the simple structure of the edge states (2.10) and (2.12) also changes significantly: each edge state is a four-component vector for $\gamma \neq 0$. Because of that, after projecting the impurity matrix (2.16) onto the edge state subspace we get the dimensionless coupling matrix $\mathcal{J}_{ij}$ which typically has all nine non-zero components instead of (2.19). This is a crucial consideration for the final formulation of the model.

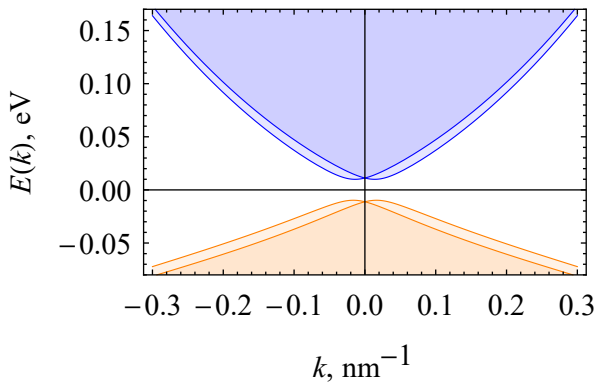

Figure 2.3: Cut of electronic energy spectrum $E(k)$ in BHZ model with the inversion asymmetry parameter $\gamma = 5$ meV. Parameters from Table 2.1 for $d = 7$ nm are used.

2.4.2 The model

For magnetic impurities in CdTe/HgTe/CdTe quantum wells inversion asymmetry complicates the dimensionless coupling matrix $\mathcal{J}_{ij}$. However, there are other reasons why the electron-impurity coupling matrix might be more complicated than that given by (2.19). First of all, in any real physical realization of a 2D TI the edge is not straight due to structural imperfections. Secondly, Kondo renormalization might generate new terms in the coupling matrix. For instance, for the four component matrix (2.19) $\mathcal{J}_{zx}$ term appears at small energy scales (see section 3.5 for details). Thirdly, not only magnetic atoms might effectively serve as magnetic impurities. As it was discussed in section 1.1, charge puddles might appear in semiconductor heterostructures. Coupling matrix for the interaction between the effective spin $S = 1/2$ of a charge puddle and the helical edge electron is given by $\mathcal{J}_{ij} = \delta_{ij}\mathcal{J}_{\text{iso}} + \delta\mathcal{J}_{ij}$, where constants $\delta\mathcal{J}_{ij}$ are much smaller than $\mathcal{J}_{\text{iso}}$ and $\delta\mathcal{J}_{ij}$ is of a general form [17, 18]. Finally, even if magnetic atoms are considered, the coupling matrix given by (2.19) is specific for CdTe/HgTe/CdTe quantum wells, which implies that for other 2D TI the coupling matrix might be of a different form.

For the mentioned reasons in the following sections we consider the general Hamiltonian

$$H = H_0 + H_{\text{e-i}} = -vk_y\sigma_z + \delta(y - y_0)\frac{1}{\nu}\mathcal{J}_{ij}S_i s_j. \tag{2.23}$$

For the main part of the thesis we assume that $\mathcal{J}_{ij}$ is of the general form, except for requirement $|\mathcal{J}_{ij}| \ll 1$. We note that Hamiltonian (2.23) preserves its form under rotations of the impurity: $\boldsymbol{S} \to R\boldsymbol{S}$, $\mathcal{J} \to R^T\mathcal{J}$, where $R \in SO(3)$. This implies, for instance, that matrix $\mathcal{J}$ can always be brought to lower triangular form. However, we mention that the form of Hamiltonian (2.23) is altered under rotations of the electron spin. This is due to the helical nature of the electrons at the edge of a 2D TI.

To solve the transport problem and to investigate the statistics of the backscattering current we use several additional approximations and assumptions. To begin with, we assume that the helical edge is infinite in both directions. This implies that the leads are located at $y = \pm\infty$. We assume that the temperature of both leads is T. We model the voltage applied to the leads by a difference of chemical potentials V of the edge states moving in the opposite directions. Next, we assume that a single magnetic impurity is present in the system at $y_0 = 0$. Besides, we assume that effects of Kondo renormalization are weak and that the anisotropy for the magnetic impurity is negligible. Magnetic anisotropy for $S > 1/2$, as well as Kondo renormalizations, are briefly discussed in section 3.5. Finally, we neglect electron-electron interactions.

Concluding this chapter, we present the second quantized form of the single-particle Hamilto-

nian (2.23):

$$H = iv \int dy \psi^\dagger(y) \sigma_z \partial_y \psi(y) + \frac{1}{\nu} \mathcal{J}_{ij} S_i \psi^\dagger(0) s_j \psi(0) \tag{2.24}$$

Here $\psi(y) = (\psi_\uparrow(y), \psi_\downarrow(y))^T$, $\psi^\dagger(y) = (\psi^\dagger_\uparrow(y), \psi^\dagger_\downarrow(y))$ and $\psi_{\uparrow/\downarrow}$ ($\psi^\dagger_{\uparrow/\downarrow}$) stands for the annihilation (creation) operator for the helical electrons with spin pointing up/down. To shorten the equations we will often use the following notation for the spin density operators: $\hat{s}_j(y) = \psi^\dagger(y) s_j \psi(y)$. Throughout the thesis we prefer the second quantized form (2.24) over (2.23).

Chapter 3

Generalized master equation

3.1 Introduction

As it was outlined in the introduction, our task is to investigate the backscattering current induced by a magnetic impurity located near the helical edge. Beginning this chapter, we formulate the problem in more formal terms.

We assume that voltage $V > 0$ is applied to the leads adjoined to the helical edge of a 2D TI. This implies that the chemical potential of the lead located at $y = -\infty$ is given by $\mu_- = \mu - V/2$, while the chemical potential of the lead at $y = +\infty$ is given by $\mu_+ = \mu + V/2$. In that case, because $e = -1$, the current starts to flow in y-direction along the helical edge. In the absence of magnetic impurities, the current is purely ballistic, it is given by $I_0 = (e^2/h)V$. When a single magnetic impurity is placed near the edge at $y = 0$, the ideal current I_0 is lowered, i.e. I_0 gets a small negative correction ΔI. We refer to this correction as the backscattering current. We analyze the backscattering current from different perspectives in the present and in the following chapters. From now on, we use units $e = -1$, $\hbar = 1$ so that $G_0 = e^2/h = 1/2\pi$.

Due to the specifics of helical edge electrons, there exists a compact expression determining the backscattering current [18]. In order to derive it, we note that the charge current flowing along the helical edge is always accompanied by spin polarization of the edge, as indicated by Hamiltonian (2.24). Indeed, the direction of movement of a helical electron and the direction of its spin are locked. If the positive charge current flows ($V > 0$), then more electrons move against the y-axis and, therefore, more electrons have their spin pointing up. This consideration allows us to link the backscattering current to the rate of change of z-projection of the total electron spin of the helical

edge. To this end, we introduce the second quantized operator of the latter quantity:

$$\Sigma_z = \int dy \hat{s}_z(y) = \frac{1}{2} \int dy \psi^\dagger(y) \sigma_z \psi(y). \tag{3.1}$$

Whenever Σ_z decreases by unity, a single electron is backscattered. As a consequence,

$$\Delta I = -e \frac{d\Sigma_z}{dt} = \frac{d\Sigma_z}{dt}. \tag{3.2}$$

The operator equation (3.2) is central to the thesis, we utilize it in order to investigate the backscattering current. Finishing the introduction to the present chapter, we remind the reader of the result, announced in section 2.3. Namely, it was said that if the interaction between the magnetic impurity and the helical electrons preserves the total z-projection of the angular momentum of the system, then the backscattering current is absent. This is clear from (3.2). Indeed, if z-projection of the angular momentum of the electron-impurity system is preserved, then Σ_z can maximally change by $2S$ and, consequently, cannot accumulate with time. For this reason, momentum non-conserving processes are of uttermost importance in the considered problem.

3.2 Cumulant generating function

We are interested in the zero-frequency behavior of the backscattering current. In this regard, we calculate the statistics of the number of backscattered electrons during the time interval t. We introduce the operator of the latter quantity as

$$\Delta N(t) = \Sigma_z(t) - \Sigma_z(0). \tag{3.3}$$

In this expression the time dependence is introduced through the Heisenberg representation for the operator Σ_z:

$$\Sigma_z(t) = e^{iHt} \Sigma_z e^{-iHt}, \tag{3.4}$$

where H is given by (2.24). As a next step, we need to introduce the cumulant generating function $G(\lambda)$. However, there is a difference between how it is done for classical and for quantum systems. In the classical case $G(\lambda)$ is given by the expression

$$G(\lambda, t) = \ln\langle e^{i\lambda \Delta N(t)} \rangle = \ln\langle e^{i\lambda \Sigma_z(t) - i\lambda \Sigma_z(0)} \rangle. \tag{3.5}$$

Here $\Sigma_z(t)$ and $\Sigma_z(0)$ are simple numbers and the average is taken over all possible configurations of the system. In that case, the cumulants can be calculated as

$$\langle\langle \Delta N^n(t)\rangle\rangle = \langle\langle [\Sigma_z(t) - \Sigma_z(0)]^n\rangle\rangle = (-i)^n \left(\partial/\partial\lambda\right)^n G(\lambda, t). \tag{3.6}$$

However, in the quantum case the expression for the cumulant generating function is more complicated. The main reason for that is the noncommutativity of $\Sigma_z(t)$ operator at different times. The proper way to introduce $G(\lambda, t)$ is [36]

$$G(\lambda, t) = \ln \mathrm{Tr}\left[e^{i\lambda\Sigma_z(t)} e^{-i\lambda\Sigma_z(0)} \rho(0)\right]. \tag{3.7}$$

In this expression $\rho(0)$ is the initial density matrix of the whole system (the edge electrons and the impurity). Equation (3.7) is valid provided that $\rho(0)$ commutes with $\Sigma_z(0) = \Sigma_z$. We assume $\rho(0)$ is given by

$$\rho(0) = \rho_S(0) \otimes \frac{\exp\left[-\beta \int dy \psi^\dagger(y) \left(i\sigma_z v \partial_y - \sigma_z V/2 - \mu\right) \psi(y)\right]}{\mathrm{Tr}_e \exp\left[-\beta \int dy \psi^\dagger(y) \left(i\sigma_z v \partial_y - \sigma_z V/2 - \mu\right) \psi(y)\right]}. \tag{3.8}$$

Here $\rho_S(0) = \frac{1}{2S+1} I_{(2S+1)\times(2S+1)}$, Tr_e denotes the trace over all electronic states, and $\beta = 1/T$ is the inverse temperature of the leads. In that case, $\rho(0)$ and Σ_z indeed commute and we can utilize formula (3.7). We assume that the duration t of the considered time interval is sufficiently long so that the impurity has time to relax to its steady state and to backscatter a large number of electrons afterwards. Next, we note that the generating function (3.7) can be rewritten as

$$G(\lambda, t) = \ln \mathrm{Tr}\left[e^{iH^{-\lambda}t} e^{-iH^{\lambda}t} \rho(0)\right], \qquad H^\lambda = e^{i\frac{\lambda}{2}\Sigma_z} H e^{-i\frac{\lambda}{2}\Sigma_z}. \tag{3.9}$$

In other words, to evaluate the cumulant generating function we need to consider the evolution of the system on a closed Keldysh contour. The Keldysh partition function is non-trivial due to the presence of a quantum field $\pm\Sigma_z$ which has a plus sign on the forward branch of the Keldysh contour and a minus sign on the backward branch. To proceed, we rewrite (3.9) in a slightly different manner:

$$G(\lambda, t) = \ln \mathrm{Tr}\rho^\lambda(t). \tag{3.10}$$

Here $\rho^\lambda(t)$ satisfies

$$\frac{d\rho^\lambda(t)}{dt} = -iH^\lambda \rho^\lambda(t) + i\rho^\lambda(t) H^{-\lambda}, \qquad \rho^\lambda(0) = \rho(0). \tag{3.11}$$

Therefore, in order to calculate $G(\lambda)$ and investigate the statistics of the backscattering current, one has to track the non-Hermitian evolution of the system governed by equation (3.11). We will use representation (3.10) for $G(\lambda)$ throughout the thesis.

3.3 Generalized master equation

Although now we have compact equations (3.10) and (3.11) that determine the generating function, using these equation to extract any physical results seems to be a formidable task. The problem comes from the fact that the considered system has a macroscopically large number of degrees of freedom. However, with the use of perturbation theory in electron-impurity coupling $\mathcal{J}_{ij}$ it is possible to reduce the problem to the $(2S+1)$-dimensional Hilbert space of the magnetic impurity. The first step towards this goal is to rewrite

$$G(\lambda, t) = \ln \mathrm{Tr}\rho^{\lambda}(t) = \ln \mathrm{Tr}_S \mathrm{Tr}_e \rho^{\lambda}(t) = \ln \mathrm{Tr}_S \rho_S^{\lambda}(t). \tag{3.12}$$

Therefore, to study the cumulant generating function, we need to derive the master equation for the reduced density matrix $\rho_S^{\lambda}(t) = \mathrm{Tr}_e \rho^{\lambda}(t)$ of the magnetic impurity. As long as $\lambda \neq 0$ we call this master equation generalized.

3.3.1 Mean-field part of the electron-impurity interaction

We start the derivation of the generalized master equation for the magnetic impurity by referring to the explicit form of Hamiltonian (2.24). A crucial thing to notice is that the electron-impurity interaction Hamiltonian $H_{\mathrm{e-i}} = \mathcal{J}_{ij} S_i \hat{s}_j(0)/\nu$ has a non-zero expectation value over the unperturbed density matrix (3.8). Indeed, for the average spin operator we get $\langle \hat{s}_j \rangle_0 = \mathrm{Tr}_e \left(\rho(0)\hat{s}_j(0)\right) = \nu V \delta_{jz}/2$, where V is the voltage applied to the leads. The appearance of a non-zero $\langle \hat{s}_z(0) \rangle$ is expected, because, as it was discussed, charge current along the edge of a 2D TI is always associated with spin polarization of the edge. We conclude that the interaction Hamiltonian obtains a finite expectation

$$H_{\mathrm{e-i}}^{\mathrm{mf}} = \langle H_{\mathrm{e-i}} \rangle_0 = \mathcal{J}_{iz} V S_i/2. \tag{3.13}$$

It can be seen that the voltage bias effectively breaks time-reversal symmetry for the magnetic impurity: finite V leads to Zeeman splitting of the impurity levels. In that case, it is clear that the mean-field part of the electron-impurity interaction Hamiltonian should be treated separately. We

denote the "irreducible" part of the electron-impurity interaction as

$$\mathcal{V} = H_{\mathrm{e-i}} - H^{\mathrm{mf}}_{\mathrm{e-i}} = \frac{1}{\nu}\mathcal{J}_{ij}S_i\hat{s}_j - \frac{1}{\nu}\mathcal{J}_{ij}S_i\langle\hat{s}_j\rangle_0 = \frac{1}{\nu}\mathcal{J}_{ij}S_i : \hat{s}_j : . \tag{3.14}$$

In this expression and onwards, we do not specify the position of the impurity: $\hat{s}_j(0) \to \hat{s}_j$. This makes derivations less bulky without causing any confusion as, by assumption, there is only one impurity in the system. Note that we introduced an "irreducible" spin density operator $: \hat{s}_j :$.

3.3.2 Perturbative approach to the generalized master equation

At the present stage, we have the following master equation:

$$\frac{d\rho^{\lambda}(t)}{dt} = -i[H_0 + H^{\mathrm{mf}}_{\mathrm{e-i}}, \rho^{\lambda}(t)] - i\mathcal{V}^{\lambda}\rho^{\lambda}(t) + i\rho^{\lambda}(t)\mathcal{V}^{-\lambda}, \qquad e^{i\frac{\lambda}{2}\Sigma_z}\mathcal{V}e^{-i\frac{\lambda}{2}\Sigma_z}. \tag{3.15}$$

To obtain (3.15) from (3.11) we used the fact that Σ_z commutes with H_0 and with $H^{\mathrm{mf}}_{\mathrm{e-i}}$. As a next step in the derivation of the generalized master equation, we go to the interaction picture with the respect to the Hamiltonian $H_0 + H^{\mathrm{mf}}_{\mathrm{e-i}}$:

$$\frac{d\rho^{\lambda}_I(t)}{dt} = -i\mathcal{V}^{\lambda}_I(t)\rho^{\lambda}_I(t) + i\rho^{\lambda}_I(t)\mathcal{V}^{-\lambda}_I(t). \tag{3.16}$$

The idea behind the following evaluation is to trace out the electronic degrees of freedom and to get the equation for $\rho^{\lambda}_S(t)$. However, straightforward application of Tr_e to equation (3.16) is not meaningful unless there is a clear way to utilize the perturbation theory. In order to allow for the perturbative treatment, we formally solve (3.16):

$$\rho^{\lambda}_I(t) = \rho(0) - i\int_0^t dt' \left(\mathcal{V}^{\lambda}_I(t')\rho^{\lambda}_I(t') - \rho^{\lambda}_I(t')\mathcal{V}^{-\lambda}_I(t')\right). \tag{3.17}$$

Then we substitute the result back into (3.16). This gives

$$\frac{d\rho^{\lambda}_I(t)}{dt} = -i\mathcal{V}^{\lambda}_I(t)\rho(0) + i\rho(0)\mathcal{V}^{-\lambda}_I(t) + \int_0^t dt' \left(\mathcal{V}^{\lambda}_I(t')\rho^{\lambda}_I(t')\mathcal{V}^{-\lambda}_I(t) + \mathcal{V}^{\lambda}_I(t)\rho^{\lambda}_I(t')\mathcal{V}^{-\lambda}_I(t')\right) - \\ - \int_0^t dt' \left(\mathcal{V}^{\lambda}_I(t)\mathcal{V}^{\lambda}_I(t')\rho^{\lambda}_I(t') + \rho^{\lambda}_I(t')\mathcal{V}^{-\lambda}_I(t')\mathcal{V}^{-\lambda}_I(t)\right). \tag{3.18}$$

Expression (3.18) is more suitable than (3.16) for tracing out electrons. We apply Tr_e to the both parts of equation (3.18). Immediately, we see that both averages $\mathrm{Tr}_e\left(\mathcal{V}^{\lambda}_I(t)\rho(0)\right)$ and $\mathrm{Tr}_e\left(\rho(0)\mathcal{V}^{-\lambda}_I(t)\right)$

nullify, because $\mathcal{V}$ contains only irreducible operators of the electron system. Therefore,

$$\frac{d\rho^{\lambda}_{S,I}(t)}{dt} = \mathrm{Tr}_e\left[\int_0^t dt' \left(\mathcal{V}^{\lambda}_I(t')\rho^{\lambda}_I(t')\mathcal{V}^{-\lambda}_I(t) + \mathcal{V}^{\lambda}_I(t)\rho^{\lambda}_I(t')\mathcal{V}^{-\lambda}_I(t')\right)\right] - \\ -\mathrm{Tr}_e\left[\int_0^t dt' \left(\mathcal{V}^{\lambda}_I(t)\mathcal{V}^{\lambda}_I(t')\rho^{\lambda}_I(t') + \rho^{\lambda}_I(t')\mathcal{V}^{-\lambda}_I(t')\mathcal{V}^{-\lambda}_I(t)\right)\right]. \tag{3.19}$$

Throughout the thesis, we use the second order perturbation theory in $\mathcal{J}_{ij}$ (renormalizations aside). We note that the right hand side of equation (3.19) is already of the second order in $\mathcal{J}_{ij}$. This allows us to use Born approximation: $\rho^{\lambda}_I(t) \approx \rho^{\lambda}_{S,I}(t) \otimes \rho_0$, where $\rho_0 = \mathrm{Tr}_S\left(\rho(0)\right)$. The corrections to Born approximation produce only higher-order terms in $\mathcal{J}_{ij}$ [36]. Therefore, the trace in equation (3.19) can be explicitly calculated. In order to outline the general calculation strategy, let us focus on the first term in the right hand side of equation (3.19). We will refer to this terms as I_1. Other terms can be processed in the similar fashion. We begin with explicitly substituting the expression for $\mathcal{V}$:

$$I_1 = \mathrm{Tr}_e\left[\int_0^t dt' \left(\mathcal{V}^{\lambda}_I(t')\rho^{\lambda}_I(t')\mathcal{V}^{-\lambda}_I(t)\right)\right] = \frac{\mathcal{J}_{ik}\mathcal{J}_{jp}}{\nu^2}\int_0^t dt' S_{i,I}(t')\rho^{\lambda}_{S,I}(t')S_{j,I}(t)\mathcal{C}^{\lambda,-\lambda}_{kp}(t-t') \tag{3.20}$$

Here $\mathcal{C}^{\lambda,-\lambda}_{kp}(t-t')$ stands for spin-spin correlation function of the helical edge electrons:

$$\mathcal{C}^{\lambda,-\lambda}_{kp}(t-t') = \mathrm{Tr}_e\left[: \hat{s}^{-\lambda}_{p,I}(t) :: \hat{s}^{\lambda}_{k,I}(t') : \rho_0\right]. \tag{3.21}$$

Interaction representation for spin operators is defined by

$$S_{i,I}(t) = e^{iH^{\mathrm{mf}}_{\mathrm{e-i}}t}S_i e^{-iH^{\mathrm{mf}}_{\mathrm{e-i}}t}, \qquad : \hat{s}^{\lambda}_{k,I}(t) := e^{iH_0 t}e^{i\frac{\lambda}{2}\Sigma_z} : \hat{s}_k : e^{-i\frac{\lambda}{2}\Sigma_z}e^{-iH_0 t}. \tag{3.22}$$

The order of the exponents does not matter in the latter expression because $[\Sigma_z, H_0] = 0$. Straightforward calculation shows that

$$\hat{s}^{\lambda}_k = e^{i\frac{\lambda}{2}\Sigma_z}\hat{s}_k e^{-i\frac{\lambda}{2}\Sigma_z} = R^{\lambda}_{kr}\hat{s}_r, \qquad R^{\lambda} = \begin{pmatrix} \cos\frac{\lambda}{2} & -\sin\frac{\lambda}{2} & 0 \\ \sin\frac{\lambda}{2} & \cos\frac{\lambda}{2} & 0 \\ 0 & 0 & 1 \end{pmatrix}. \tag{3.23}$$

We conclude that

$$\mathcal{C}^{\lambda,-\lambda}_{kp}(\tau) = R^{\lambda}_{kr}\mathcal{C}_{rl}(\tau)R^{-\lambda}_{pl} = R^{\lambda}_{kr}\mathcal{C}_{rl}(\tau)R^{\lambda}_{lp}, \qquad \mathcal{C}_{rl}(\tau) = \mathcal{C}^{0,0}_{rl}(\tau). \tag{3.24}$$

Correlation function $\mathcal{C}_{rl}(\tau)$ decays exponentially at large times. The energy scale of the decay is controlled by either voltage or temperature, the only energy scales associated with the helical edge electrons. At the same time, $\rho^{\lambda}_{S,I}(t)$ changes at much larger times due to small $\mathcal{J}_{ik}\mathcal{J}_{jp}$ multiplier in the master equation. We conclude that the memory effects are not important for the dynamics of the magnetic impurity and Markov approximation $\rho_{S,I}(t') \approx \rho_{S,I}(t)$ can be applied. Moreover, at sufficiently large t, the lower integration limit in (3.19) can be prolonged to $-\infty$. In that case, expression (3.20) for I_1 can be rewritten as

$$I_1 = \frac{\mathcal{J}_{ik}\mathcal{J}_{jp}}{\nu^2} R^{\lambda}_{kr} R^{-\lambda}_{pl} \int_0^{\infty} d\tau S_{i,I}(t-\tau)\rho^{\lambda}_{S,I}(t) S_{j,I}(t)\mathcal{C}_{rl}(\tau). \tag{3.25}$$

Next we introduce the eigenbasis of the mean-field Hamiltonian $H^{\text{mf}}_{\text{e-i}}$: $|m\rangle$, where m corresponds to the projection of the impurity spin in the direction of the effective Zeeman field, $m = +S, ..., -S$. We denote the corresponding energies as E_m. Trivial calculation shows that

$$E_m = m\sqrt{\mathcal{J}^2_{xz} + \mathcal{J}^2_{yz} + \mathcal{J}^2_{zz}}V/2.$$

With that in mind we can rewrite

$$S_{i,I}(t-\tau) = e^{iH^{\text{mf}}_{\text{e-i}}t}\left[\sum_{mn} e^{i\omega_{mn}\tau}\mathcal{S}^{mn}_i\right]e^{-iH^{\text{mf}}_{\text{e-i}}t}, \qquad \mathcal{S}^{mn}_i = |m\rangle S^{mn}_i\langle n|, \qquad \omega_{mn} = E_n - E_m. \tag{3.26}$$

Therefore, I_1 is brought to the following form:

$$I_1 = \frac{\mathcal{J}_{ik}\mathcal{J}_{jp}}{\nu^2} R^{\lambda}_{kr} R^{-\lambda}_{pl} e^{iH^{\text{mf}}_{\text{e-i}}t}\left[\sum_{mn}\mathcal{C}_{rl}(\omega_{mn})\mathcal{S}^{mn}_i\rho^{\lambda}_S(t)S_j\right]e^{-iH^{\text{mf}}_{\text{e-i}}t}, \tag{3.27}$$

where $\mathcal{C}_{rl}(\omega_{mn}) = \int_0^{\infty} d\tau e^{i\omega_{mn}\tau}\mathcal{C}_{rl}(\tau)$. To proceed further, we decompose the correlation function in the following way:

$$\mathcal{C}_{rl}(\omega_{mn}) = \frac{1}{2}\gamma_{rl}(\omega_{mn}) + i\mathcal{A}_{rl}(\omega_{mn}), \qquad \gamma^{\dagger} = \gamma, \qquad \mathcal{A}^{\dagger} = \mathcal{A}. \tag{3.28}$$

The anti-Hermitian part of the correlation function produces terms in the generalized master equation that, represented as integrals over energy, diverge in the ultraviolet limit. These divergent contributions are known to renormalize the Hamiltonian of the system [37]. For now, we will ignore them. We will systematically discuss the renormalizations in section 3.5. The Hermitian part

is given by

$$\gamma_{rl}(\omega) = \frac{\pi\nu^2}{2}\sum_{\sigma_1\sigma_2}\sigma_l^{\sigma_1\sigma_2}\sigma_r^{\sigma_2\sigma_1}\int d\xi n_F(\xi-\sigma_1 V/2)\left[1-n_F(\xi+\omega-\sigma_2 V/2)\right], \tag{3.29}$$

where $n_F(\epsilon) = 1/(e^{\beta(\epsilon-\mu)}+1)$ and $\sigma_{1/2} = \pm 1$. Straightforward evaluation of the integrals leads to $\gamma(\omega) = \nu^2\Pi(\omega) = \nu^2(\Pi^+(\omega)+\Pi^-(\omega))$ with

$$\Pi^{\pm}(\omega) = \frac{\pi T}{2}\begin{pmatrix} f(\omega\pm V) & \mp i f(\omega\pm V) & 0 \\ \pm i f(\omega\pm V) & f(\omega\pm V) & 0 \\ 0 & 0 & f(\omega)\end{pmatrix}, \quad f(\omega) = \beta\omega/(1-e^{-\beta\omega}). \tag{3.30}$$

Let us denote[1] the typical value of $|\mathcal{J}_{ij}|$ as $\mathcal{J}$. In that case, $\omega = \omega_{mn} \sim \mathcal{J}V$. If $V \ll T$, then $\omega_{mn} \ll T$ and ω_{mn} can be omitted in the correlation functions. If, on the contrary, $V \gg T$, then $\gamma_{33}(\omega_{mn})$ can be neglected in comparison to the other elements of γ. At the same time, $\omega_{mn} \ll V$ and $f(\omega_{mn}\pm V) \approx f(\pm V)$. Therefore, with the required precision we can always neglect ω_{mn} in the correlation functions. This allows us to sum $\mathcal{S}_i^{mn}$ in equation (3.27) into S_i. We conclude that

$$I_1 = \frac{1}{2}\eta_{ij}^{\lambda,-\lambda} e^{iH_{\mathrm{e-i}}^{\mathrm{mf}}t}\left[S_i\rho_S^{\lambda}(t)S_j\right]e^{-iH_{\mathrm{e-i}}^{\mathrm{mf}}t}, \qquad \eta_{ij}^{\lambda,-\lambda} = \left(\mathcal{J}R^{\lambda}\Pi(0)R^{\lambda}\mathcal{J}^T\right)_{ij} \tag{3.31}$$

We note that $\Pi(0)$ is given be the following simple matrix:

$$\Pi(0) = \pi T\begin{pmatrix} \frac{V}{2T}\coth\frac{V}{2T} & -i\frac{V}{2T} & 0 \\ i\frac{V}{2T} & \frac{V}{2T}\coth\frac{V}{2T} & 0 \\ 0 & 0 & 1\end{pmatrix}. \tag{3.32}$$

Expression (3.31) is the final form of I_1, the first term in equation (3.19). All other terms can be processed similarly. In order to write down the final result for the master equation, we go back to Schrödinger picture. Moreover, we introduce $\eta = \eta^{0,0}$. In that case, the generalized master equation that determines the statistics of the backscattering current is given by

$$\frac{d\rho_S^{\lambda}(t)}{dt} = -i[H_{\mathrm{e-i}}^{\mathrm{mf}}, \rho_S^{\lambda}(t)] + \eta_{ij}\left(S_i\rho_S^{\lambda}(t)S_j - \{\rho_S^{\lambda}(t), S_jS_i\}/2\right) + (\eta_{ij}^{\lambda,-\lambda}-\eta_{ij})S_i\rho_S^{\lambda}(t)S_j. \tag{3.33}$$

Equation (3.33) is the central result of the present chapter.

[1] $\mathcal{J}$ as a number will be used only in the numerical estimates. Therefore, we believe that this notation is not confusing.

3.3.3 Superoperator form of the generalized master equation

In order to determine the cumulant generating function of the backscattering current $G(\lambda, t)$ we note that equation (3.33) can be brought to the superoperator form:

$$\frac{d}{dt}\left(\rho_S^\lambda(t)\right)_{mn} = \mathcal{L}^\lambda_{mn,kp}\left(\rho_S^\lambda(t)\right)_{kp}, \qquad m,n,k,p = S,...,-S. \tag{3.34}$$

Here the evolution superoperator $\mathcal{L}^\lambda$ does not depend on time. We order the eigenvalues of $\mathcal{L}^\lambda$ from the one with the largest real part to the one with the lowest real part: ϵ_1^λ, ϵ_2^λ,...,$\epsilon^\lambda_{(2S+1)^2}$. In that case, it is clear that in the large time limit the cumulant generating function is given by

$$G(\lambda, t) = \ln \mathrm{Tr}_S\left(\rho_S^\lambda(t)\right) = t\epsilon_1^\lambda. \tag{3.35}$$

In terms of superoperator algebra, usual trace operation Tr_S corresponds to scalar product of a given vector with a vector δ_{mn}. Therefore, in (3.35) we implicitly assumed that the vector corresponding to the eigenvalue ϵ_1^λ is not orthogonal to δ_{mn}. This is typically the case. Therefore, the final approach to the problem of calculation of the cumulants of the number of backscattered electrons is the following:

$$\frac{\langle\langle \Delta N^k \rangle\rangle}{t} = \left(-i\frac{\partial}{\partial\lambda}\right)^k \epsilon_1^\lambda. \tag{3.36}$$

Before using (3.36) to investigate the behaviour of the backscattering current, we discuss the master equation at $\lambda = 0$ and the renormalizations that appear in the problem.

3.4 Dynamics of the magnetic impurity

In this section we consider the case $\lambda = 0$. When $\lambda = 0$ the master equation simply describes the dynamics of the magnetic impurity mediated by its interaction with the surrounding helical edge electrons. We find that the generalized master equation (3.33) is reduced to [20]

$$\frac{d\rho_S(t)}{dt} = -i[H^{\mathrm{mf}}_{\mathrm{e-i}}, \rho_S(t)] + \eta_{ij}\left(S_i\rho_S(t)S_j - \{\rho_S(t), S_jS_i\}/2\right). \tag{3.37}$$

Equation (3.37) has a standard Lindbladian form [36, 37]. This guarantees the conservation of probability in the course of time evolution. In terms of the superoperator language, there exists a left eigenvector δ_{mn} of a superoperator $\mathcal{L}^{\lambda=0}_{mn,kp}$ corresponding to a zero eigenvalue. Existence of a zero eigenvalue implies that equation (3.37) has a steady state solution (right eigenvector corresponding to zero eigenvalue). Moreover, we conclude that $\epsilon_1^{\lambda=0} = 0$. Other eigenvalues $\epsilon_i^{\lambda=0}$

have a negative real part, they describe the process of relaxation of the magnetic impurity due to its interaction with helical edge electrons. The corresponding real parts define the relaxation rates. We note that in principle helical edge electrons might be not the only cause of spin relaxation for magnetic impurities in real materials. For example, spin-lattice relaxation might take place. Still, we neglect such effects focusing on the relaxation processes induced by electron-impurity interaction.

As a next step, we discuss different terms in equation (3.37). The mean-field term in the master equation (3.37) describes the unitary evolution of the state of the magnetic impurity. Physically, it drives the precession of the magnetic impurity around the direction of Zeeman mean-field $\propto \mathcal{J}_{iz}V$ (3.13). We remind that our considerations require[2] $\mathcal{J} \ll 1$ so that the mean-field is much smaller than the voltage whenever the discussed theory is applicable. The term in (3.37) proportional to η is responsible for the relaxation of the state of the magnetic impurity. It can be estimated as $\eta \sim \mathcal{J}^2 \max(V, T)$.

The appearance of two energy scales demonstrates that there are two distinct regimes for the magnetic impurity. If $V \ll \mathcal{J}T$ then the mean-field term in (3.37) is much smaller than the relaxation term. In that case, the mean-field is completely irrelevant and can be safely neglected. As the voltage is increased the mean-field becomes more and more important for the dynamics of the impurity. For $V \gg \mathcal{J}T$ the mean-field term is dominant and the density matrix of the magnetic impurity tends to be diagonal in the eigenbasis of $H^{\mathrm{mf}}_{\mathrm{e-i}}$. We note that the relaxation term cannot be neglected even for very large voltages.

Finishing this subsection, we mention that equation (3.37) can be further simplified in the limit $V \gg \mathcal{J}T$, i.e. when the relaxation term in (3.37) is much smaller than the mean-field term. Physically, this limit corresponds to the case when the energy levels of the magnetic impurity are smeared only weakly by the relaxation. This allows for the use of the rotating wave approximation (RWA). First, we go back to the interaction picture:

$$\frac{d\rho_{S,I}(t)}{dt} = \eta_{ij}\left(S_{i,I}(t)\rho_{S,I}(t)S_{j,I}(t) - \{\rho_{S,I}(t), S_{j,I}(t)S_{i,I}(t)\}/2\right). \tag{3.38}$$

Then we represent $\rho_{S,I} = \sum_{mn} p_{mn}|m\rangle\langle n|$, where $|m\rangle$, $|n\rangle$ are the eigenstates of H^{mf}_{e-i}. We find

$$\frac{dp_{cd}}{dt} = \sum_{mn} \eta_{ij}\left(e^{i(\omega_{mc}+\omega_{dn})t}S_i^{cm}p_{mn}S_j^{nd} - e^{i\omega_{mc}t}(S_jS_i)^{cm}p_{mn}\delta_{nd}/2 - e^{i\omega_{dn}t}(S_jS_i)^{nd}p_{mn}\delta_{mc}/2\right). \tag{3.39}$$

Using RWA means throwing away quickly oscillating terms in (3.39). This can be done whenever

[2]From now on we often refer to the typical value of $\mathcal{J}_{ij}$ elements as $\mathcal{J} > 0$.

$V \gg \mathcal{J}T$. Moreover, we note that in general S_i^{cm} is not zero only if $c = m, m \pm 1$. Then we see that the equation for the evolution of diagonal elements of p_{mn} decouples from the equation for the evolution of all other elements. We denote $p_c = p_{cc}$. In that case,

$$\frac{dp_c}{dt} = \sum_m \left(\eta_{ij} S_i^{cm} S_j^{mc} p_m - \eta_{ij} S_i^{mc} S_j^{cm} p_c\right), \tag{3.40}$$

while non-diagonal elements decay to zero. Equation (3.40) can be written as

$$\frac{dp_c}{dt} = \sum_m \left(p_m \omega_{m\to c} - p_c \omega_{c\to m}\right), \qquad \omega_{m\to c} = \eta_{ij} S_i^{cm} S_j^{mc}. \tag{3.41}$$

Therefore, equation (3.40) is a classical master equation that describes stochastic hopping of the magnetic impurity between different energy levels. We stress that $c = m, m \pm 1$ because otherwise spin matrix elements nullify.

3.5 Renormalizations

The divergences that appear in the derivation of the generalized master equation (3.33) are known to be common for various systems [37]. According to the general statement, while the Hermitian part of the matrix $\mathcal{C}_{rl}(\omega)$ contributes to the relaxation part of the master equation (3.33), the divergent anti-Hermitian part contributes to the unitary evolution. Therefore, the discussed divergent terms renormalize the Hamiltonian of the system. They can be classified into two categories.

Terms of the first kind diverge linearly at large energies and induce the anisotropy $\mathcal{D}_{ij} S_i S_j$ for the magnetic impurity [38]. This kind of anisotropy appears as a result of strong spin-orbit coupling in the structure. We find that $\mathcal{D}_{ij}$ is a symmetric real matrix, elements of which can be estimated as $\mathcal{J}^2\Lambda$. Here Λ is the ultraviolet cut-off for the helical edge electrons, we estimate its value as $\Lambda \sim |M|$. For $S = 1/2$ the anisotropy reduces to a constant energy shift and is, therefore, completely irrelevant. However, the dynamics of impurities with $S > 1/2$ is strongly altered by the presence of finite $\mathcal{D}_{ij}$. The magnetic anisotropy becomes irrelevant only when its energy is either much smaller than the relaxation rates of the magnetic impurity or much smaller than the energy scale dictated by the mean-field Hamiltonian (3.13). In other words, the anisotropy becomes irrelevant only when $|\mathcal{D}_{ij}| \ll \max\left(\mathcal{J}V, \mathcal{J}^2 T\right)$. We note that in principle there might be other sources of anisotropy for magnetic impurities with spin $S > 1/2$. For instance, just like helical edge states, bulk states of the quantum well might contribute to the anisotropy [32].

Terms of the second kind diverge logarithmically at large energies and are responsible for

Kondo renormalization of the coupling constants $\mathcal{J}_{ij}$ [18]. In order to treat Kondo renormalization correctly, one has to write down the one-loop renormalization group equation [18]

$$\frac{d\mathcal{J}_{ij}}{dl} = \frac{1}{2}\epsilon_{imk}\epsilon_{jnp}\mathcal{J}_{mn}\mathcal{J}_{kp}, \qquad l = \ln\left(\Lambda/E\right). \tag{3.42}$$

Here E is the running energy scale determined by $E = \max\left(V, T\right)$. We note that equation (3.42) is valid provided that $\mathcal{J} \ll 1$ and that $\max(V, T) \gg |\mathcal{D}_{ij}|$. At $\mathcal{J} \sim 1$ the one-loop approximation fails. At energies smaller than $|\mathcal{D}_{ij}|$ the renormalization group equation alters significantly [39]. Equation (3.42) can be brought to a simple form by utilizing singular-value decomposition of the coupling matrix: $\mathcal{J} = R_{<}QR_{>}$ [20]. In this expression matrices $R_{>/<} \in SO(3)$ and $Q = \mathrm{diag}\left(q_1, q_2, q_3\right)$. Diagonal elements q_1, q_2, q_3 are called singular values of $\mathcal{J}_{ij}$. We find

$$\frac{dq_1}{dl} = q_2q_3, \quad \frac{dq_2}{dl} = q_3q_1, \quad \frac{dq_3}{dl} = q_1q_2, \tag{3.43}$$

while rotation matrices $R_{>/<}$ do not flow. We find two independent integrals of motion: $\mathcal{I}_1 = q_1^2 - q_2^2$ and $\mathcal{I}_2 = q_2^2 - q_3^2$. If $q_1 = q_2 = 0$, q_3 does not change. If $q_1 = q_2 \neq 0$, $q_3 \leq 0$, and $|q_1| \leq |q_3|$ then q_1 goes to zero while q_3 saturates at some finite value with the decrease of E. The latter scenario includes the ferromagnetic case $q_1 = q_2 = q_3 < 0$. Otherwise, a finite Kondo energy scale E_K exists at which q_i diverge. As E_K is approached, the coupling constants tend to the manifold $|q_1| = |q_2| = |q_3|$ with $q_1q_2q_3 > 0$. The renormalization group flow for $q_1 = q_2$ is depicted in Figure 3.1.

To demonstrate how the coupling matrix can change under renormalization group flow, we consider the specific case of the four component coupling matrix (2.18). We see that additionally to $\mathcal{J}_{xx}$, $\mathcal{J}_{yy}$, $\mathcal{J}_{zz}$, and $\mathcal{J}_{xz}$ elements of the coupling matrix, $\mathcal{J}_{zx}$ element appears when the energy scale is changed:

$$\mathcal{J} = \begin{pmatrix} \mathcal{J}_{xx} & 0 & \mathcal{J}_{xz} \\ 0 & \mathcal{J}_{yy} & 0 \\ 0 & 0 & \mathcal{J}_{zz} \end{pmatrix} \qquad \rightarrow \qquad \mathcal{J}(E) = \begin{pmatrix} \mathcal{J}_{xx}(E) & 0 & \mathcal{J}_{xz}(E) \\ 0 & \mathcal{J}_{yy}(E) & 0 \\ \mathcal{J}_{zx}(E) & 0 & \mathcal{J}_{zz}(E) \end{pmatrix}. \tag{3.44}$$

Here $d\mathcal{J}_{zx}(E)/dl = -\mathcal{J}_{xz}(E)\mathcal{J}_{yy}(E)$. Therefore, generation of $\mathcal{J}_{zx}$ is a consequence of a joint process due to $\mathcal{J}_{yy}$ and $\mathcal{J}_{xz}$.

Throughout the main text of the thesis, we assume that the coupling constants are sufficiently small so that their renormalization can be neglected at relevant energy scales. We don't investigate the physics of the problem at $E \lesssim E_K$. For discussion of the latter case see [18]. Still, weak

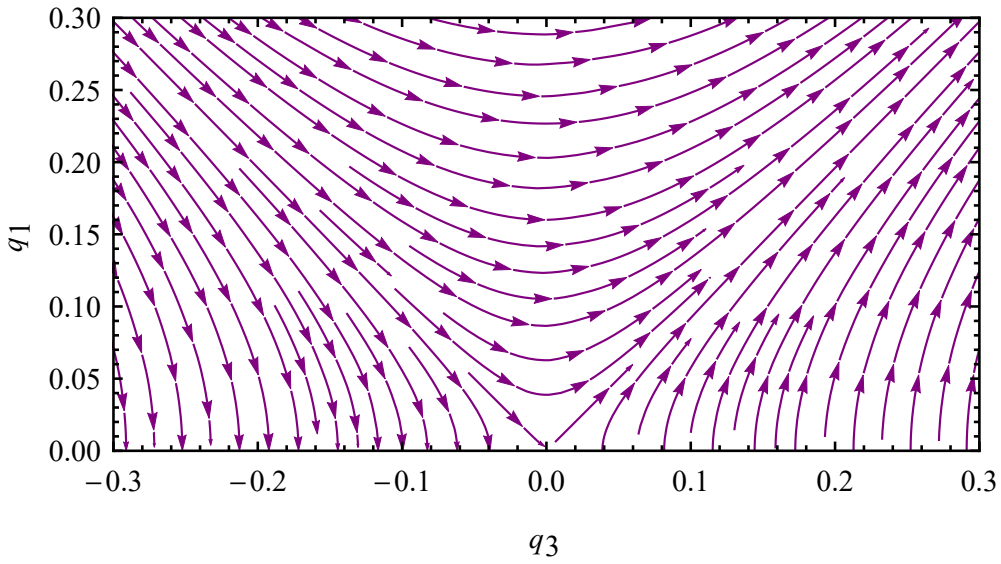

Figure 3.1: Renormalization group flow for singular values q_i of the coupling matrix $\mathcal{J}_{ij}$ in the case $q_1 = q_2$. The flow is symmetric under $q_1 \to -q_1$. If $q_3 \leq 0$ and $|q_1| \leq |q_3|$ then $q_1 \to 0$ while q_3 saturates at some finite value at small energies. Otherwise, $q_1/q_3 \to \pm 1$, $q_3 \to +\infty$ at small energy scales.

Kondo renormalization can be easily included in the largest part of our results with the substitution $\mathcal{J}_{ij} \to \mathcal{J}_{ij}(E)$.

Now we are in the position to apply equation (3.33) to determine the statistics of backscattering current in different cases.

Chapter 4

Statistics of the backscattering current

In this chapter, we start to investigate cumulants of the backscattering current induced by the magnetic impurity located near the helical edge of 2D TI. Using the generalized master equation (3.33), we derived:

- The general formula that relates average backscattering current to spin averages in the steady state. This general formula is valid for impurities with arbitrary spin S.
- The steady state density matrix of the impurity with arbitrary S in the case $V \gg \mathcal{J}T$. It can be utilized, for example, to calculate the average current.

Moreover, we obtained several results that are specific for magnetic impurities with spin $S = 1/2$. We derived:

- Exact expressions for the average backscattering current and for its dispersion. These expressions are valid at arbitrary voltage.
- Explicit formula for the generating function of the number of backscattered electrons in the case $V \gg \mathcal{J}T$.

4.1 Magnetic impurity with arbitrary spin: average backscattering current

In this section, we discuss the average backscattering current ΔI for the magnetic impurity with arbitrary spin. To derive the corresponding equations, we investigate the eigenvalue ϵ_1^λ of the superoperator $\mathcal{L}^\lambda_{mn,kp}$. Then, the average number of backscattered electrons is determined by the first order term in the expansion of ϵ_1^λ over λ, as indicated by (3.36). We apply the first-order

perturbation theory in λ to determine the required coefficient. As the unperturbed superoperator we take $\mathcal{L}^0_{mn,kp}$ and then we consider $\Delta\mathcal{L}^\lambda_{mn,kp} = \mathcal{L}^\lambda_{mn,kp} - \mathcal{L}^0_{mn,kp}$ as a perturbation.

For the unperturbed superoperator $\mathcal{L}^0_{mn,kp}$ the eigenvalue $\epsilon^0_1 = 0$. Let l_{mn} be the left eigenvector of $\mathcal{L}^0_{mn,kp}$ corresponding to this eigenvalue and r_{kp} - the right eigenvector. Then, to get the first order correction due to the perturbation, one has to multiply $\Delta\mathcal{L}^\lambda_{mn,kp}$ by the l_{mn} from the left and by r_{kp} from the right. Moreover, $\Delta\mathcal{L}^\lambda_{mn,kp}$ should be expanded up to the first order in λ. As it was discussed in chapter 3, the left eigenvector $l_{mn} = \delta_{mn}$, while the right eigenvector r_{kp} is given by the steady state density matrix of the master equation (3.37), which we denote as $\rho^{(\mathrm{st})}_S$. Therefore,

$$\Delta I = \langle \Delta N \rangle / t = l_{mn} \frac{\partial \Delta \mathcal{L}^\lambda_{mn,kp}}{\partial(i\lambda)} r_{kp} = \frac{\partial \Delta \mathcal{L}^\lambda_{mm,kp}}{\partial(i\lambda)} \rho^{(\mathrm{st})}_{S,kp}, \qquad \lambda = 0. \tag{4.1}$$

Using the generalized master equation (3.33), we find

$$\begin{gathered} \Delta I = -\left(\mathcal{J} Q \mathcal{J}^T\right)_{ij} \langle S_j S_i \rangle, \qquad \langle S_j S_i \rangle = \mathrm{Tr}_S \left[S_j S_i \rho^{(\mathrm{st})}_S \right], \\ Q_{xx} = Q_{yy} = \pi T \frac{V}{2T}, \qquad Q_{xy} = -Q_{yx} = -i\pi T \frac{V}{2T} \coth \frac{V}{2T}, \qquad Q_{iz} = Q_{zi} = 0. \end{gathered} \tag{4.2}$$

Note that the matrix $\left(\mathcal{J} Q \mathcal{J}^T\right)_{ij}$ is positive definite so that the correction to the backscattering current is always negative. This is in accordance with common sense. Explicit calculation shows

$$\Delta I = \frac{\pi}{4} V \left(\chi_r \langle S_r \rangle \coth \frac{V}{2T} - 2 \sum_{k=x,y} \mathcal{J}_{ik} \mathcal{J}_{jk} \langle S_i S_j \rangle \right), \qquad \chi_r = 2\epsilon_{rij} \mathcal{J}_{ix} \mathcal{J}_{jy}. \tag{4.3}$$

If we introduce the conductance quantum $G_0 = 1/2\pi$ ($e = -1$ and $\hbar = 1$), then the backscattering correction to the conductance reads

$$\Delta G = \frac{\Delta I}{V} = \frac{\pi^2}{2} G_0 \left(\chi_r \langle S_r \rangle \coth \frac{V}{2T} - 2 \sum_{k=x,y} \mathcal{J}_{ik} \mathcal{J}_{jk} \langle S_i S_j \rangle \right). \tag{4.4}$$

At the first glance, the presence of $\coth V/2T$ may seem surprising due to its divergence at small voltages. However, $\langle S_r \rangle \propto V$ at small voltage $V \ll T$, and backscattering conductance ΔG is finite. We mention that ΔG is of the second order in $\mathcal{J}_{ij}$ which is consistent with Fermi's golden rule.

4.1.1 Small voltage regime

Equations (4.3) and (4.4) relate the backscattering current to the steady state density matrix of the magnetic impurity. However, in the limit $V \ll T$ one can compute the average ΔI without

calculating the full density matrix. The main idea is that at small voltages we can change

$$\langle S_i S_j \rangle \approx \frac{S(S+1)}{3}\delta_{ij}. \tag{4.5}$$

Therefore, only spin averages $\langle S_r \rangle$ in the steady state are required to calculate the backscattering current. For $V \ll T$ it is possible to obtain a closed equation for these spin averages. We start from the equation for the density matrix in the steady state. According to (3.37), it reads

$$-i[H^{\text{mf}}_{\text{e-i}}, \rho^{(\text{st})}] + \eta_{ij}\left(S_i \rho^{(\text{st})} S_j - \{\rho^{(\text{st})}, S_j S_i\}/2\right) = 0 \tag{4.6}$$

Multiplying (4.6) by S_k, taking trace, and applying (4.5) for all terms already proportional to voltage, we obtain

$$\langle S_r \rangle = \frac{V}{T}\frac{S(S+1)}{3}\Gamma^{-1}_{rk}\chi_k, \qquad \Gamma_{kr} = \frac{1}{\pi T}\left(\text{Tr}\,(\eta)\,\delta_{kr} - \frac{\eta_{kr}+\eta_{rk}}{2} + V\mathcal{J}_{iz}\epsilon_{ikr}\right). \tag{4.7}$$

The latter term in the expression for Γ_{kr} appears due to the mean-field term in (4.6). We note that in the considered limit $V \ll T$ the formula for Γ_{kr} simplifies to

$$\Gamma_{kr} = \text{Tr}\left(\mathcal{J}\mathcal{J}^T\right)\delta_{kr} - \left(\mathcal{J}\mathcal{J}^T\right)_{kr} + \frac{V}{\pi T}\mathcal{J}_{iz}\epsilon_{ikr}. \tag{4.8}$$

Substituting the expression for $\langle S_r \rangle$ from (4.7) into (4.4) we obtain

$$\Delta G = -\frac{S(S+1)}{3}\pi^2 G_0\left(g - \chi_r \Gamma^{-1}_{rk}\chi_k\right), \qquad g = K_{xx} + K_{yy}, \qquad K = \mathcal{J}^T\mathcal{J}. \tag{4.9}$$

Note that in the limit $V \ll T$ the only spin dependence in the answer comes from the the multiplier $S(S+1)$. We mention that Γ_{kr} changes its form radically at $V \sim \mathcal{J}T$, i.e. when all terms in (4.8) are of the same order. This leads to the crossover behaviour in the conductance at $V \sim \mathcal{J}T$. We underline that the result (4.9) respects the aforementioned $SO(3)$ symmetry $\mathcal{J} \to R^T\mathcal{J}$.

In the intermediate voltage regime $\mathcal{J}T \ll V \ll T$ it is possible to further simplify expression (4.9). To this end, we utilize the fact that in the expression (4.8) for Γ_{kr} the dominant term is the noninvertible mean-field contribution $\propto \mathcal{J}V/T$. Therefore, the general task we face is the inversion of the matrix of the following kind:

$$c_{kr} = a_{kr} + b_i\epsilon_{ikr}, \qquad |b_i| \gg |a_{kr}|. \tag{4.10}$$

One can easily check that in the leading order in a/b the inverse matrix is given by

$$c_{rk}^{-1} \approx \frac{b_r b_k}{b_i a_{ij} b_j}. \tag{4.11}$$

Another thing to note is that $\chi_r \mathcal{J}_{rz} = 2\text{det}\mathcal{J}$. Therefore, we conclude that for $\mathcal{J}T \ll V \ll T$

$$\Delta G = -\frac{S(S+1)}{3}\pi^2 G_0 \left(g - \frac{4\text{det}K}{gK_{zz} - K_{zx}^2 - K_{zy}^2} \right). \tag{4.12}$$

Finally, we note that for $S = 1/2$ expression (4.12) is valid at any voltage $V \gg \mathcal{J}T$, i.e. there is no restriction from above at $V \sim T$. That happens because for $S = 1/2$ the anticommutator $\{S_i, S_j\} \propto \delta_{ij}$. However, for higher S it is impossible to simplify double-spin averages and (4.12) fails at $V \sim T$. For this reason, the backscattering current for $S > 1/2$ has two crossovers: the first one at $V \sim \mathcal{J}T$ and the second one at $V \sim T$.

We once again stress out that the backscattering current nullifies, whenever the electron-impurity interaction preserves z-projection of the total spin of the system. This can be seen in the formulas (4.9) and (4.12). Let us suppose that the coupling matrix $\mathcal{J}_{ij}$ is diagonal. Then for $V \ll T$ we get

$$\Delta G = -\frac{S(S+1)}{3}\pi^2 G_0 \frac{\left(\mathcal{J}_{xx}^2 - \mathcal{J}_{yy}^2\right)^2}{\mathcal{J}_{xx}^2 + \mathcal{J}_{yy}^2}. \tag{4.13}$$

Electron-impurity interaction conserves z-projection of the angular momentum if $\mathcal{J}_{xx} = \mathcal{J}_{yy}$. We see that in that case ΔI indeed nullifies. Another interesting aspect of (4.13) is the absence of a crossover at $V \sim \mathcal{J}T$. The crossover appears if, for example, we add $\mathcal{J}_{xz}$ component to the matrix.

4.1.2 Steady state density matrix and high voltage regime

For arbitrary value of the impurity spin it is impossible to represent the backscattering current in a compact form (4.9) at high voltages $V \gtrsim T$. However, it is possible to derive a simple expression for the steady state density matrix of the magnetic impurity valid for $V \gg \mathcal{J}T$. After that, obtained $\rho_S^{(\text{st})}$ can substituted into (4.4) in order to calculate the backscattering current in the regime $V \gtrsim T$. The resultant expression for the current is bulky for arbitrary S and casts no transparent physical meaning. For this reason, we do not present the final formula in the thesis. Still, it is enlightening to follow the derivation of the steady state density matrix for $V \gg \mathcal{J}T$. Results of this subsection have a huge significance for the remainder of the text.

First of all, we note that at $V \gg \mathcal{J}T$ the steady state density matrix is diagonal in the eigenbasis of the mean-field Hamiltonian (3.13). Therefore, to simplify the calculations, we can rotate

the basis to align the mean-field with z-direction. This is automatically achieved if we bring the electron-impurity coupling matrix to lower-triangular form. We introduce

$$\boldsymbol{S} = R\boldsymbol{S}', \qquad \mathcal{J} = R^T\mathcal{J}', \qquad \mathcal{J}' = \begin{pmatrix} \mathcal{J}'_{xx} & 0 & 0 \\ \mathcal{J}'_{yx} & \mathcal{J}'_{yy} & 0 \\ \mathcal{J}'_{zx} & \mathcal{J}'_{zy} & \mathcal{J}'_{zz} \end{pmatrix}. \tag{4.14}$$

Then, the mean-field term in the Hamiltonian reads

$$H^{\text{mf}}_{\text{e-i}} = \frac{V}{2}\mathcal{J}'_{zz}S'_z. \tag{4.15}$$

The eigenstates of this Hamiltonian are $|m\rangle = |S'_z = m\rangle, m = +S, ..., -S$. The steady state density matrix is diagonal in $|m\rangle$ basis: $\rho_S^{(\text{st})} = \sum_m p_m^{(\text{st})}|m\rangle\langle m|$. In order to determine the occupation probabilities $p_m^{(\text{st})}$ in the steady state we rewrite equation (3.40) as

$$\frac{dp_c}{dt} = \sum_m \left(\eta'_{ij}S_i'^{cm}S_j'^{mc}p_m - \eta'_{ij}S_i'^{mc}S_j'^{cm}p_c\right) = 0, \qquad \eta' = R^T\eta R = \mathcal{J}'\Pi(0)\mathcal{J}'^T. \tag{4.16}$$

In the matrix form this equation reads

$$\frac{dp_c}{dt} = \sum_m L^0_{ca}p_m. \tag{4.17}$$

In a single hop process for the magnetic impurity S'_z can change only by unity. Therefore, the matrix L^0 is tridiagonal. Its exact form is

$$L^0_{cm} = \begin{cases} \eta'_+(S(S+1) - m(m+1))/4, & c = m+1 \\ \eta'_-(S(S+1) - m(m-1))/4, & c = m-1 \\ -L^0_{m+1,m} - L^0_{m-1,m}, & c = m \end{cases}, \qquad \eta'_\pm = (\eta'_{xx} \pm i\eta'_{xy}) \mp i(\eta'_{yx} \pm i\eta'_{yy}). \tag{4.18}$$

The latter case ($c = m$) represents the probability conservation $\sum_c p_c = 1$ (we assume that $L^0_{S+1,S}$ and $L^0_{-S-1,-S}$ nullify). We proceed with task of finding the steady state density matrix. The direct check shows that

$$p_m^{(\text{st})} = \frac{\vartheta^m}{\mathcal{Z}}, \qquad \mathcal{Z} = \sum_{m=-S}^{S}\vartheta^m, \qquad \vartheta = \frac{\eta'_+}{\eta'_-}. \tag{4.19}$$

We note that the steady state is of the Gibbsian form. Equation (4.19) allows us to write down the

final expression for the density matrix:

$$\rho_S^{(\mathrm{st})} = \frac{1}{\mathcal{Z}} \exp\left(S'_z \ln \vartheta\right) = \frac{1}{\mathcal{Z}} \exp\left(R^T_{zk} S_k \ln \vartheta\right). \tag{4.20}$$

Gibbsian parameter ϑ can simplified to

$$\vartheta = \frac{\left[(\mathcal{J}'_{xx})^2 + (\mathcal{J}'_{yy})^2 + (\mathcal{J}'_{yx})^2\right] \coth V/2T + 2\mathcal{J}'_{xx}\mathcal{J}'_{yy}}{\left[(\mathcal{J}'_{xx})^2 + (\mathcal{J}'_{yy})^2 + (\mathcal{J}'_{yx})^2\right] \coth V/2T - 2\mathcal{J}'_{xx}\mathcal{J}'_{yy}}. \tag{4.21}$$

We note that the under the proper choice of the rotation matrix R the product $\mathcal{J}'_{xx}\mathcal{J}'_{yy}$ might be assumed to be positive. This implies that the state with $S'_z = +S$ is the most populated in the steady state. Whenever referring to the lower triangular form of the coupling matrix $\mathcal{J}$ we will assume that this is the case. We parametrize ϑ as

$$\vartheta = \frac{\coth V/2T + \sqrt{B}}{\coth V/2T - \sqrt{B}} \geq 1, \qquad B = \frac{4(\mathcal{J}'_{xx})^2(\mathcal{J}'_{yy})^2}{\left[(\mathcal{J}'_{xx})^2 + (\mathcal{J}'_{yy})^2 + (\mathcal{J}'_{yx})^2\right]^2}, \qquad 0 \leq B \leq 1. \tag{4.22}$$

We note that at $B = 0$ the Gibbsian parameter $\vartheta = 1$ and all states are equally populated at any voltage. At the same time, in the case $B = 1$ the impurity becomes fully polarized for $V \gg T$. Therefore, parameter B controls the polarization of the impurity at high voltage $V \gg T$. This parameter will be of uttermost importance in the subsequent sections of the thesis. We mention that if the electron-impurity coupling matrix preserves angular momentum in the z-direction (in that case z-direction is not altered by the rotation R), the parameter $B = 1$. It is possible to check that B can be written in the rotationally invariant form:

$$B = \frac{4K_{zz}\mathrm{det}K}{(gK_{zz} - K_{zx}^2 - K_{zy}^2)^2}. \tag{4.23}$$

Here $K = \mathcal{J}^T\mathcal{J}$ is the same matrix that appeared in (4.9) and (4.12). Formula (4.23) is indeed invariant under left rotations $R \in SO(3)$ of the coupling matrix: if $\mathcal{J} \to R^T\mathcal{J}$, then $K \to K$. Note that combination similar to B also enters the expression (4.12) for the conductance in the intermediate regime $\mathcal{J}T \ll V \ll T$. This is not a coincidence, as it will be shown later.

4.2 Statistics of the backscattering current for spin-1/2 magnetic impurity

In this section, we consider only the case $S = 1/2$. We obtain the general expression for the dispersion of the number of electrons $\langle\langle \Delta N^2 \rangle\rangle$ backscattered by the magnetic impurity during time interval t. This quantity is equivalent to the zero-frequency noise of the backscattering current ΔI. Moreover, we derive the cumulant generating function $G(\lambda)$ in the case $V \gg \mathcal{J}T$.

The main idea of the section is that the density matrix for $S = 1/2$ can be decomposed into the impurity spin operators:

$$\rho_S^\lambda(t) = \beta_k(t) S_k, \qquad k = 0, 1, 2, 3. \tag{4.24}$$

Note that $\mathrm{Tr}_S \rho_S^\lambda(t) = 2\beta_0(t)$. We mention that decomposition (4.24) cannot be applied to magnetic impurities with $S > 1/2$. The generalized master equation (3.33) can be written in the following form:

$$\frac{d}{dt}\beta_k = \mathcal{M}_{kp}^\lambda \beta_p. \tag{4.25}$$

Here matrix $\mathcal{M}^\lambda$ can be represented as

$$\mathcal{M}^\lambda = \begin{pmatrix} \mathcal{M}_{00}^\lambda & \mathcal{M}_{0n}^\lambda \\ \mathcal{M}_{m0}^\lambda & \mathcal{M}_{mn}^\lambda \end{pmatrix} = \begin{pmatrix} W^\lambda & U_n^\lambda \\ V_m^\lambda & Z_{mn}^\lambda \end{pmatrix}, \qquad m, n = 1, 2, 3. \tag{4.26}$$

Before writing down the explicit form of W^λ, U_n^λ, V_m^λ, and Z_{mn}^λ we introduce two functions:

$$T_1^\lambda = 2\cos\frac{\lambda}{2}\left(\coth\frac{V}{2T}\cos\frac{\lambda}{2} - i\sin\frac{\lambda}{2}\right), \qquad T_2^\lambda = 2\sin\frac{\lambda}{2}\left(\coth\frac{V}{2T}\sin\frac{\lambda}{2} + i\cos\frac{\lambda}{2}\right). \tag{4.27}$$

Then the explicit calculation shows that

$$\begin{aligned} U_n^\lambda &= i\frac{\pi V}{16}\chi_n T_1^\lambda \tan\frac{\lambda}{2}, \qquad V_m^\lambda = -i\frac{\pi V}{4}\chi_m T_2^\lambda \cot\frac{\lambda}{2}, \\ W^\lambda &= -\frac{\pi V}{8} g T_2^\lambda, \qquad Z_{mn}^\lambda = -\frac{\pi T}{2}\Gamma_{mn} - \frac{\pi V}{4} Q_{mn} T_2^\lambda. \end{aligned} \tag{4.28}$$

We remind that Γ is given by equation (4.7), $g = K_{xx} + K_{yy}$, $K = \mathcal{J}^T\mathcal{J}$. Moreover, we used a new notation:

$$Q_{mn} = \mathcal{J}_{mx}\mathcal{J}_{nx} + \mathcal{J}_{my}\mathcal{J}_{ny} - \frac{g}{2}\delta_{mn}. \tag{4.29}$$

Note that $W^{\lambda=0} = 0$ and $U_n^{\lambda=0} = 0$ which guarantees trace preservation for $\lambda = 0$. Our goal is to find the eigenvalue ϵ_1^λ of $\mathcal{M}^\lambda$ with the largest real part. In order to do that, we need to solve the

secular equation

$$\det\left(\mathcal{M}^{\lambda}-\epsilon^{\lambda}I_{4\times4}\right)=0. \tag{4.30}$$

This equation is equivalent to

$$\left(W^{\lambda}-\epsilon^{\lambda}-U_n^{\lambda}\left(Z^{\lambda}-\epsilon^{\lambda}I_{3\times3}\right)^{-1}_{nm}V_n^{\lambda}\right)\det\left(Z^{\lambda}-\epsilon^{\lambda}I_{3\times3}\right)=0. \tag{4.31}$$

We know that $\epsilon_1^{\lambda=0}=0$ so the overall determinant should be zero at $\lambda=0$. However, det$Z^{\lambda=0}\neq0$. Therefore, the equation we investigate further is

$$W^{\lambda}-\epsilon^{\lambda}-U_n^{\lambda}\left(Z^{\lambda}-\epsilon^{\lambda}I_{3\times3}\right)^{-1}_{nm}V_n^{\lambda}=0. \tag{4.32}$$

In fact, this equation contains the information about all four eigenvalues of the matrix $\mathcal{M}^{\lambda}$.

4.2.1 Zero-frequency noise

We substitute $t\epsilon_1^{\lambda}\approx i\lambda\langle\Delta N\rangle-\lambda^2\langle\langle\Delta N^2\rangle\rangle/2$ into equation (4.32). Expanding the overall expression up to the second order in λ we find $\langle\Delta N\rangle$ and $\langle\langle\Delta N^2\rangle\rangle$. The first cumulant is given by

$$\Delta I=\frac{\langle\Delta N\rangle}{t}=-\frac{\pi V}{8}\left(g-\frac{V}{2T}\coth\frac{V}{2T}\chi_r\Gamma^{-1}_{rk}\chi_k\right). \tag{4.33}$$

Equation (4.33) coincides with (4.9) taken at $S=1/2$. Presence of $\coth V/2T$ must not disturb the reader: for $V\gg\mathcal{J}T$ it cancels with $\coth V/2T$ coming from Γ^{-1}_{rk}. To verify this one needs to use (4.11). Therefore, $(V/2T)\coth V/2T$ multiplier can be safely omitted at all voltages. More crucially, we get the expression for the zero-frequency noise of the backscattering current:

$$\begin{aligned}\frac{\langle\langle\Delta N^2\rangle\rangle}{t}=\frac{\pi T}{4}\left(\frac{V}{2T}\coth\frac{V}{2T}g-\frac{V^2}{4T^2}\left(1+\coth^2\frac{V}{2T}\right)\chi_r\Gamma^{-1}_{rk}\chi_k-\right.\\ \left.-\frac{V^3}{8T^3}\coth\frac{V}{2T}\chi_r\Gamma^{-1}_{rk}\left(2Q_{kp}+\delta_{kp}\frac{V}{2T}\coth\frac{V}{2T}\chi_i\Gamma^{-1}_{ij}\chi_j-\delta_{kp}g\right)\Gamma^{-1}_{pl}\chi_l\right)\end{aligned} \tag{4.34}$$

It is especially important to consider limit $V\ll T$. In that case the third term in the brackets can be neglected and (4.34) reduces to

$$\frac{\langle\langle\Delta N^2\rangle\rangle}{t}=\frac{\pi T}{4}\left(g-\chi_r\Gamma^{-1}_{rk}\chi_k\right)=-2T\Delta G,\qquad\Delta G=\Delta I/V \tag{4.35}$$

This equation is the manifestation of the fluctuation-dissipation theorem. Note that the result (4.35) is non-trivial, because the correction to conductance ΔG depends on voltage even at small voltages

$V \ll T$, showing a crossover behaviour at $V \sim \mathcal{J}T$.

If we are interested in the limit $V \gg \mathcal{J}T$, than we can simplify equations (4.33) and (4.34) by using (4.11) as it was done when obtaining (4.12) from (4.9). We use parameter B, defined earlier in equations (4.22) and (4.23). Moreover, we introduce a new parameter C which is defined as

$$C = 1 - \frac{K_{zx}^2 + K_{zy}^2}{gK_{zz}}. \tag{4.36}$$

In terms of the lower-triangular form $\mathcal{J}'$ of the coupling matrix (4.14) parameter C can be written as

$$C = \frac{(\mathcal{J}'_{xx})^2 + (\mathcal{J}'_{yy})^2 + (\mathcal{J}'_{yx})^2}{(\mathcal{J}'_{xx})^2 + (\mathcal{J}'_{yy})^2 + (\mathcal{J}'_{yx})^2 + (\mathcal{J}'_{zx})^2 + (\mathcal{J}'_{zy})^2}. \tag{4.37}$$

Note that both B and C lay from 0 to 1. If the electron-impurity interaction preserves z-projection of the total angular momentum of the system, then both B and C are equal to unity. We note that the backscattering current in the limit $V \gg \mathcal{J}T$ is given by

$$\Delta I = \frac{\langle \Delta N \rangle}{t} = -\frac{\pi g V}{8}(1 - BC). \tag{4.38}$$

The correction to the current indeed nullifies for $B = C = 1$. Zero-frequency noise can be expressed as

$$\frac{\langle\langle \Delta N^2 \rangle\rangle}{t} = \frac{\pi g V}{8} \tanh \frac{V}{2T} \left(1 - B^2 C + \frac{1 - BC}{\sinh^2 V/2T} \right). \tag{4.39}$$

Crucially, zero-frequency noise has a crossover from $\langle\langle \Delta N^2 \rangle\rangle \propto T$ to $\langle\langle \Delta N^2 \rangle\rangle \propto V$ at $V \sim T$. We will investigate this equation in more details in Chapter 5. Now we proceed with the calculation of the cumulant generating function of the backscattering current for $V \gg \mathcal{J}T$.

4.3 The full counting statistics

In the general case, when the ratio between voltage and temperature is arbitrary, it is impossible to evaluate the full counting statistics of the backscattering current. Still, if the mean-field term in the master equation (3.37) is much larger than the relaxation term, i.e. $V \gg \mathcal{J}T$, it possible to determine the whole cumulant generating function $G(\lambda)$ or, at least, its behavior at moderately small λ. In the present section, we discuss the respective derivation and highlight the criteria of the validity for the obtained answers. The central equation for this subsection is (4.32).

The main problem we face is inversion of the matrix $Z^\lambda - \epsilon^\lambda I_{3\times 3}$ in equation (4.32). If we were to explicitly invert this matrix, we would get a fourth order equation for ϵ_λ that cannot be

straightforwardly solved. However, the simplification comes from the fact that we are interested in the root ϵ_1^λ for which $\epsilon_1^{\lambda=0} = 0$. In that case, the mean-field term $\propto \mathcal{J}V$ in Γ dominates in the expression for Z^λ at $V \gg \mathcal{J}T$ (see equation (4.28) for details). This allows us to use the matrix inversion trick (4.11) and get a quadratic equation for ϵ^λ. The corresponding roots are given by

$$\epsilon^\lambda = -\frac{\pi g V}{8} \coth\frac{V}{2T}\left((1-C)P_\lambda + C\left[1 \mp \sqrt{1+(B-1)\left(P_{2\lambda} - \frac{\sin^2\lambda}{\cosh^2(V/2T)}\right)}\right]\right). \tag{4.40}$$

In this expression we introduced

$$P_\lambda = 1 - \cos\lambda + i\tanh\frac{V}{2T}\sin\lambda. \tag{4.41}$$

One can see that the root nullifying at $\lambda = 0$ corresponds to minus sign in expression (4.40). At the moment, we know two solutions of (4.28), they are both $\propto \mathcal{J}^2 \max(V,T)$. Two other solutions are non-zero at $\lambda = 0$ and have a large imaginary part $\propto \mathcal{J}V$ that corresponds to quick rotation in the mean-field. We will briefly describe these roots for $V \gg T$ later.

In any case, we get the expression for the cumulant generating function, that is valid at least for small λ:

$$\epsilon_1^\lambda = -\frac{\pi g V}{8} \coth\frac{V}{2T}\left((1-C)P_\lambda + C\left[1 - \sqrt{1+(B-1)\left(P_{2\lambda} - \frac{\sin^2\lambda}{\cosh^2(V/2T)}\right)}\right]\right). \tag{4.42}$$

This equation can be utilized to find all finite cumulants $\langle\langle \Delta N^n \rangle\rangle/t$: they can be calculated according to (3.36). For example, expanding the generating function (4.42) up to the second order in λ, we immediately get equation (4.33) for average backscattering current and equation (4.39) for zero-frequency noise. We note that each sine and cosine function entering expression (4.42) can be decomposed into exponents $e^{-i\lambda}$ and $e^{i\lambda}$. In that case, terms $\propto e^{-i\lambda}$ correspond to regular backscattering processes that reduce the current flowing along the helical edge. At the same time, terms $\propto e^{i\lambda}$ correspond to scattering processes that induce a positive contribution to the current. The latter processes are induced by thermal fluctuations. Indeed, all terms $\propto e^{i\lambda}$ in the cumulant generating function (4.42) disappear in the limit $V \gg T$.

When investigating the backscattering processes it is generally a good idea to get rid of thermal fluctuations by applying large voltage V. Therefore, in the remainder of the text we focus on the regime $V \gg T$.

4.3.1 Cumulant generating function in the high voltage regime

We start the discussion by simplifying the cumulant generating function (4.42) for $V \gg T$. First of all, we note that in the considered limit $P_\lambda = 1 - e^{-i\lambda}$. In other words, P_λ is proportional to the cumulant generating function of an ideal Poisson backscattering process. Overall, we obtain

$$\epsilon_1^\lambda = -\frac{\pi g V}{8}\left((1-C)(1-e^{-i\lambda}) + C\left[1 - \sqrt{1-(1-B)(1-e^{-2i\lambda})}\right]\right). \tag{4.43}$$

In order to elucidate the physical meaning of the generating function (4.43) we switch to the lower triangular form $\mathcal{J}'$ of the electron-impurity coupling matrix $\mathcal{J}$ (4.14). We remind that in this case

$$B = \frac{4(\mathcal{J}'_{xx})^2(\mathcal{J}'_{yy})^2}{\left[(\mathcal{J}'_{xx})^2 + (\mathcal{J}'_{yy})^2 + (\mathcal{J}'_{yx})^2\right]^2}, \quad C = \frac{(\mathcal{J}'_{xx})^2 + (\mathcal{J}'_{yy})^2 + (\mathcal{J}'_{yx})^2}{(\mathcal{J}'_{xx})^2 + (\mathcal{J}'_{yy})^2 + (\mathcal{J}'_{yx})^2 + (\mathcal{J}'_{zx})^2 + (\mathcal{J}'_{zy})^2}.$$

Both parameters B and C lay from zero to unity. As it was mentioned, B describes polarization of the magnetic impurity in the steady state for $V \gg T$ (see (4.22) for details). If $B = 0$, then the impurity is not polarized, it occupies all of its states with equal probability. At the same time, $B = 1$ corresponds to the full polarization of the impurity along z-direction (in the rotated basis).

Parameter C describes the relative weight of different processes of electron-impurity interaction. Processes, associated with $\mathcal{J}'_{xx}$, $\mathcal{J}'_{yy}$, and $\mathcal{J}'_{yx}$ are responsible for processes in which impurity spin-flips are accompanied with electron spin-flips. Therefore, each time spin of the impurity flips due to these processes, a single electron is backscattered (at $V \gg T$). On the contrary, coupling constants $\mathcal{J}'_{zx}$ and $\mathcal{J}'_{zy}$ induce backscattering processes, that are not accompanied with impurity spin-flips. In this processes the magnetic impurity is effectively frozen, i.e. it behaves in a classical way. From these considerations, we conclude that backscattering processes with no impurity spin-flips are prohibited ($\mathcal{J}'_{zx} = \mathcal{J}'_{zy} = 0$) if parameter $C = 1$. At the same time, if $C = 0$, then $\mathcal{J}'_{xx} = \mathcal{J}'_{yy} = \mathcal{J}'_{yx} = 0$ and the impurity is fully classical, i.e. no backscattering processes lead to the flipping of the impurity spin.

To clarify the physical meaning of (4.43) we stick to the limit $1 - B \ll 1$. In that case we can expand the square root and obtain

$$\epsilon_1^\lambda = -\frac{\pi g V}{8}\left((1-C)(1-e^{-i\lambda}) + \frac{1}{2}C(1-B)(1-e^{-2i\lambda})\right). \tag{4.44}$$

Equation (4.44) implies that if the magnetic impurity is almost fully polarized, then the resultant backscattering process is a sum of independent single-particle Poisson backscattering and pairwise Poisson backscattering. Backscattering in pairs can be easily explained qualitatively, as it was done

in [29]. The main idea is that the pairing of electrons happens due to processes of simultaneous electron and impurity spin-flips. First of all, the magnetic impurity backscatters a single electron, hopping from $|S'_z = 1/2\rangle$ to $|S'_z = -1/2\rangle$. However, when the impurity is almost fully polarized ($1 - B \ll 1$), the occupation of the latter state is very improbable and the impurity immediately hops back. This leads to reflection of another electron. Overall, a pair is reflected. The discussed contribution to the cumulant generating function indeed nullifies when $\mathcal{J}'_{xx} = \mathcal{J}'_{yy} = \mathcal{J}'_{yx} = 0$, i.e. $C = 0$.

Single-electron Poisson backscattering happens due to processes associated with $\mathcal{J}'_{zx}$ and $\mathcal{J}'_{zy}$ coupling constants. As we discussed, these processes lead to classical backscattering of electrons that is not accompanied with impurity spin-flips. Therefore, single-electron Poisson nature of the backscattering is not surprising. Importantly, rate of scattering due to processes induced by $\mathcal{J}'_{zx}$ and $\mathcal{J}'_{zy}$ is $\propto {S'_z}^2$, as indicated by Fermi's golden rule (the corresponding terms in the Hamiltonian are $\mathcal{J}'_{zx} S'_z \hat{s}_x$ and $\mathcal{J}'_{zy} S'_z \hat{s}_y$). Therefore, the rate is constant for magnetic impurities with $S = 1/2$. Later we will demonstrate that the dependence of scattering rate on S_z will lead to a crucial difference in statistics of backscattering for magnetic impurities with $S > 1/2$. Finally, we note that single-electron contribution nullifies when $\mathcal{J}'_{zx} = \mathcal{J}'_{zy} = 0$, i.e. $C = 1$.

At smaller $B \lesssim 1$ the cumulant generating function (4.43) for the backscattering current still can be decomposed into the single-electron part and two-electron part. While single-particle part describes a Poisson process for arbitrary B, statistics of two-electron reflections becomes less trivial due to long-time correlations.

4.3.2 Additional roots of the secular equation

Finishing the present chapter, we discuss additional roots of equation (4.32) for $V \gg T$. As it was mentioned previously, (4.43) works well provided we are interested in sufficiently small λ. However, at larger λ solution for the generating function might alter. First of all, we note that for $B < 1/2$ the square root in (4.43) becomes ambiguous at points $\lambda = \pi/2$ and $\lambda = 3\pi/2$. Therefore, one has to be careful when choosing the branch of the square root. A more subtle issue comes from two additional roots of equation (4.32). It is possible to check that these roots are given by

$$\epsilon^\lambda = \pm i \frac{V}{2} \sqrt{K_{zz}} - \frac{\pi g V}{8} \left[2 - C - (1 - C)(1 - e^{-i\lambda}) \right]. \tag{4.45}$$

Note that the imaginary part for these two roots is always parametrically larger than the real part. The large imaginary part appears due to the mean-field term in the generalized master equation (3.33). One can verify that additional roots are important only when $C < 2/3$. Moreover, the real

part of these roots is larger than the real part of (4.43) only in the regime $|\lambda - \pi| \leq \lambda_C$, where $0 \leq \lambda_C \leq \pi/2$.

To sum up, for $C > 2/3$ and $B > 1/2$ the cumulant generating function for any λ is given by (4.43). Otherwise, equation (4.43) gives $G(\lambda)$ for $\lambda < \pi/2$, while for $\lambda > \pi/2$ one has to be more careful when calculating the cumulant generating function. However, the respective analysis is beyond the scope of the present thesis.

Chapter 5

Fano factor of the backscattering current

In this chapter, we continue to study the statistics of the backscattering current, induced by the magnetic impurity at the edge of a 2D TI. We stick to the limit $V \gg T$ in which thermal fluctuations of the backscattering current can be omitted. One of the principal goals of the chapter is to analyse magnetic impurities with arbitrary spin S. Keeping this in mind, we restrict our analysis to the first two cumulants of the number of backscattered electrons ΔN. The main results we obtained are the following:

- We calculated the Fano factor of the backscattering current for $S = 1/2$ for arbitrary structure of the electron-impurity coupling matrix $\mathcal{J}_{ij}$. We proved that the Fano factor lies strictly between 1 and 2, generalizing the result of [29].
- We demonstrated that for any S the Fano factor can be expressed as a function of two dimensionless parameters B and C.
- We analyzed the Fano factor for arbitrary S in the limit $1 - B \ll 1$, i.e. when the magnetic impurity is almost fully polarized.
- We analyzed the Fano factor for arbitrary S in the limit $B \ll 1$, i.e. when the magnetic impurity is completely smeared over all of its levels.
- Based on the limiting cases, we qualitatively described the behavior of the Fano factor for arbitrary S, C, and B.

5.1 General remarks

In our problem, we define the Fano factor of the backscattering current as the following ratio:

$$F = -\frac{\langle\langle \Delta N^2 \rangle\rangle}{\langle \Delta N \rangle}, \qquad V \gg T. \tag{5.1}$$

Both cumulants $\langle \Delta N \rangle$ and $\langle\langle \Delta N^2 \rangle\rangle$ of the backscattering current scale linearly with time. This implies that the Fano factor is a constant number. We underline that the Fano factor is defined for the backscattering current ΔI and not for the total current.

Generally speaking, the Fano factor gives the information about the correlations in the process of electron backscattering. It has a transparent physical meaning: F estimates the number of subsequent electrons that backscatter in a correlated way. For example, if the backscattering of helical edge electrons is a single-electron Poisson process, then $F = 1$. If electrons backscatter in pairs and reflection of pairs is a Poisson process, then $F = 2$. For three-electron Poisson backscattering $F = 3$ and so on. Throughout this chapter we will stick to the lower triangular form $\mathcal{J}'$ of the coupling matrix $\mathcal{J}$. For this reason, in the remainder of the thesis we omit all primes. Instead of using $\mathcal{J}'$, we simply assume that

$$\mathcal{J} = \begin{pmatrix} \mathcal{J}_{xx} & 0 & 0 \\ \mathcal{J}_{yx} & \mathcal{J}_{yy} & 0 \\ \mathcal{J}_{zx} & \mathcal{J}_{zy} & \mathcal{J}_{zz} \end{pmatrix}. \tag{5.2}$$

This will not cause any confusion, because all of the results for the Fano factor will be expressed through rotationally invariant dimensionless quantities B and C. Rotationally invariant definitions of these parameters are presented in (4.23) and (4.36) respectively. Alternative expressions for B and C in terms of the lower triangular form of the coupling matrix are presented in (4.22) and (4.37). We remind the reader of the physical meaning of B and C. Parameter B satisfies $0 \leq B \leq 1$ and describes the polarization of the magnetic impurity at $V \gg T$. Indeed, according to (4.22), the Gibbs parameter ϑ can be expressed through B in the following way:

$$\vartheta = \frac{1 + \sqrt{B}}{1 - \sqrt{B}}, \qquad V \gg T. \tag{5.3}$$

Therefore, $B = 0$ means that the impurity is equally distributed among its states, while $B = 1$ corresponds to a fully polarized magnetic impurity. Parameter C also satisfies $0 \leq C \leq 1$. It describes the importance of electron scattering processes, that occur without the impurity spin-flips.

For $C = 0$ each electron backscattering process leads to the impurity spin-flip, while at $C = 1$ the impurity spin does not flip at all. Finally, we mention that if the electron-impurity coupling is of the lower triangular form (5.2), then the effective Zeeman mean-field $\propto \mathcal{J}V$ is aligned with the z-axis.

5.2 Fano factor for spin-1/2 magnetic impurity

According to equations (4.38) and (4.39), the Fano factor for the backscattering current in the spin-1/2 case is given by

$$F = \frac{1 - B^2 C}{1 - BC}. \tag{5.4}$$

One can easily see that for $0 \leq B, C \leq 1$, the Fano factor satisfies

$$1 \leq F \leq 2. \tag{5.5}$$

As we will see later, presence of the upper bound constitutes one of the unique features of the case $S = 1/2$. Equation (5.4) generalizes the result of [29] to the arbitrary form of the electron-impurity coupling matrix. Now we consider several particular cases. First of all, for $B = 1$ and for arbitrary C the Fano factor is strictly unity. This corresponds to a single-electron Poisson reflection of electrons from the magnetic impurity, described in subsection 4.3.1. $F = 1$ is a well expected result: indeed, according to (5.3), at $B = 1$ the dynamics of the impurity is frozen so that the impurity is effectively classical. If, on the contrary, C equals to unity, then $F = 1 + B$. Fano factor is larger than 1 because when $C = 1$ all backscattering processes are accompanied with impurity spin-flips. This leads to correlations in the reflection of subsequent electrons. If, moreover, $B \to 1$, then $F \to 2$. That means that particles reflect in independent pairs, i.e. the reflection of pairs is a Poisson process. This conclusion is consistent with (4.44). Interestingly, we can see that the precise value of the Fano factor in the point $B = C = 1$ is indeterminate because F depends on the direction in which the point is approached. Let us assume that $1 - C = \rho \cos\phi$ and $1 - B = \rho \sin\phi$, where $\rho \ll 1$. In that case, the dependence of the Fano factor on the direction ϕ is described by the following simple relation:

$$F = 2 - \frac{1}{\tan\phi + 1}. \tag{5.6}$$

The sensitivity of F to the direction ϕ is explained by the fact that the average backscattering current nullifies at $B = C = 1$, as well as all other cumulants of the number of backscattered electrons. Therefore, $B = C = 1$ is an exceptional point for F. We plot the behaviour of the Fano factor

(5.4) for different values of C and B in Figure 5.1.

5.3 Rotating wave approximation for the generalized master equation

In order to investigate the Fano factor of the backscattering current for arbitrary S we can utilize $V \gg \mathcal{J}T$ and work with a simpler classical version of the generalized master equation. Just as it was done with the master equation (3.37) at $\lambda = 0$, we use the rotating wave approximation (RWA) to simplify the problem at $\lambda \neq 0$. The resultant generalized master equation for the diagonal elements of the density matrix is

$$\frac{dp_c}{dt} = \sum_m L^\lambda_{cm} p_m, \quad c, m = +S, ..., -S. \tag{5.7}$$

Here matrix $L^\lambda = L^0 + \Delta L^\lambda$. Matrix L^0 is given by (4.18) with omitted primes. In the limit $V \gg T$, ΔL^λ reduces to

$$\Delta L^\lambda = (e^{-i\lambda} - 1)\mathcal{R}, \qquad \mathcal{R}_{cm} = \begin{cases} L^0_{cm} & c \neq m \\ \eta_{zz} c^2 & c = m \end{cases}. \tag{5.8}$$

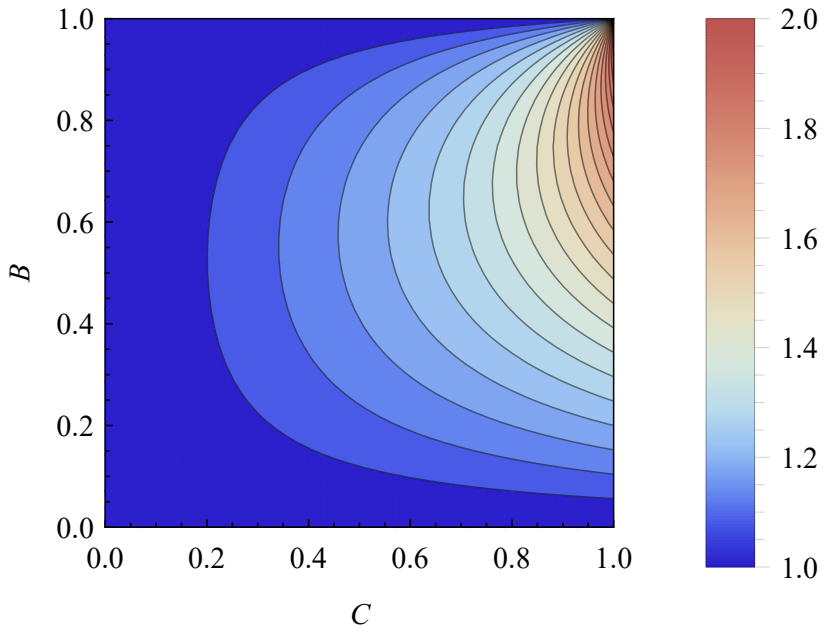

Figure 5.1: F for different values of parameters C and B in the case $S = 1/2$. Notice that the Fano factor is bounded from below and from above $1 \leq F \leq 2$.

In that case, just as it was done before, the cumulant generating function can be extracted as the eigenvalue ϵ_1^λ of the matrix L_{cm}^λ with the largest real part. For the sake of convenience, we introduce another dimensionless quantity

$$\kappa = \frac{\eta_{zz}}{\eta_-} = \frac{1}{1-\sqrt{B}}\frac{1-C}{C}. \tag{5.9}$$

Note that $\kappa = 0$ for $C = 1$ and $\kappa \to +\infty$ for $C \to 0$ as well as for $B \to 1$ at any given C.

5.3.1 Spin-1/2 case within RWA framework

It is elucidating to revisit $S = 1/2$ case, considered in the previous chapter, using RWA to obtain the cumulant generating function. The generalized master equation (5.7) reads

$$\frac{d}{dt}\begin{pmatrix} p_{+1/2} \\ p_{-1/2} \end{pmatrix} = \frac{\eta_-}{4}\begin{pmatrix} -1+\kappa(e^{-i\lambda}-1) & \vartheta e^{-i\lambda} \\ e^{-i\lambda} & -\vartheta+\kappa(e^{-i\lambda}-1) \end{pmatrix}\begin{pmatrix} p_{+1/2} \\ p_{-1/2} \end{pmatrix}. \tag{5.10}$$

Equation (5.10) has a transparent physical meaning. First of all, we note that for $V \gg T$ each impurity spin-flip leads to the backscattering of a single electron. Therefore, all impurity spin-flips should be counted when investigating the backscattering current. And that is indeed the case, as it is indicated by the presence of multiplicative counting factors $e^{-i\lambda}$ near the terms responsible for the impurity spin-flips in equation (5.10). Secondly, we see that there are terms $\kappa(e^{-i\lambda}-1)$ on the diagonal. These contributions demonstrate that even when the impurity stays in the same state, electrons can be backscattered by processes associated with the coupling constants $\mathcal{J}_{zx}$ and $\mathcal{J}_{zy}$. Using master equation (5.10) we extract the cumulant generating function.

$$\epsilon_1^\lambda = -\frac{\eta_-}{4}\left(\kappa(1-e^{-i\lambda}) + \frac{1+\vartheta}{2} - \frac{1+\vartheta}{2}\sqrt{1-\frac{4\vartheta}{(1+\vartheta)^2}(1-e^{-2i\lambda})}\right). \tag{5.11}$$

Substitution of (5.3) and (5.9) into this expression demonstrates that this result is in the full agreement with the exact generating function (4.43).

5.4 Perturbation theory for the generalized master equation

From now on we focus on magnetic impurities with large spin, i.e. we assume that $S > 1/2$. In this subsection, we find the explicit expression for the Fano factor with the help of the perturbation theory in λ.

To begin with, let us briefly recap the perturbation theory for non-Hermitian matrices and derive a general expression for the Fano factor. To this end, we consider the equation for the eigenvalue ϵ_1^λ of $L_\lambda = L_0 + \Delta L_\lambda$:

$$L^\lambda |0^\lambda\rangle\rangle = \epsilon_1^\lambda |0^\lambda\rangle\rangle. \tag{5.12}$$

Here we introduced the ket-notation $|0^\lambda\rangle\rangle$ for the right eigenvector of the matrix L^λ. Additionally, we introduce the shortened notation for the stationary state density matrix: $|0\rangle\rangle = |0^{\lambda=0}\rangle\rangle$. We remind that

$$|0\rangle\rangle = \frac{1}{\mathcal{Z}} \left(\vartheta^S, \vartheta^{S-1}, ..., \vartheta^{-S}\right)^T, \qquad \epsilon_1^{\lambda=0} = 0. \tag{5.13}$$

The left eigenvector of L^0 corresponding to $\epsilon_1^{\lambda=0} = 0$ is

$$\langle\langle\widetilde{0}| = (1, 1, ..., 1). \tag{5.14}$$

Having discussed the notations, we seek for the perturbative expansion for $|0^\lambda\rangle\rangle$ and ϵ_1^λ. We fix the normalization of $|0^\lambda\rangle\rangle$ as $\langle\langle\widetilde{0}|0^\lambda\rangle\rangle = 1$. In that case, we obtain the exact expression

$$\epsilon_1^\lambda = \langle\langle\widetilde{0}|\Delta L^\lambda|0^\lambda\rangle\rangle. \tag{5.15}$$

In order to exploit this equation further, we need to find $|0^\lambda\rangle\rangle$. Trivial algebra yields

$$L^0|0^\lambda\rangle\rangle = (\epsilon_1^\lambda - \Delta L^\lambda)|0^\lambda\rangle\rangle. \tag{5.16}$$

The matrix L^0 is not invertible since it has a zero eigenvalue. However, it may be inverted in the subspace in which the zero mode is excluded. In other words, there exists operator $\mathcal{G}$ such that

$$\mathcal{G}L^0 = 1 - |0\rangle\rangle\langle\langle\widetilde{0}|. \tag{5.17}$$

For a moment, let us assume that we know $\mathcal{G}$ and proceed further. We will construct it explicitly later. Multiplying (5.16) by $\mathcal{G}$ from the left we get

$$|0^\lambda\rangle\rangle = |0\rangle\rangle + \mathcal{G}(\epsilon_1^\lambda - \Delta L^\lambda)|0^\lambda\rangle\rangle. \tag{5.18}$$

Using Eqs. (5.15) and (5.18) the perturbation theory may be constructed in an algorithmic way. To do that, we expand

$$\Delta L^\lambda = L_1\lambda + L_2\lambda^2 + ..., \qquad \epsilon_1^\lambda = \epsilon_{1,1}\lambda + \epsilon_{1,2}\lambda^2 + ... \tag{5.19}$$

and obtain

$$\epsilon_{1,1} = \langle\langle\widetilde{0}|L_1|0\rangle\rangle, \quad \epsilon_{1,2} = \langle\langle\widetilde{0}|L_2|0\rangle\rangle - \langle\langle\widetilde{0}|L_1\mathcal{G}L_1|0\rangle\rangle. \tag{5.20}$$

Then we obtain the following expression for the Fano factor:

$$F = 2i\left(\frac{\langle\langle\widetilde{0}|L_2|0\rangle\rangle}{\langle\langle\widetilde{0}|L_1|0\rangle\rangle} - \frac{\langle\langle\widetilde{0}|L_1\mathcal{G}L_1|0\rangle\rangle}{\langle\langle\widetilde{0}|L_1|0\rangle\rangle}\right). \tag{5.21}$$

We refer to the explicit structure of ΔL_λ in the limit of large voltages. According to equation (5.8) for $V \gg T$ we have $L_1 = -i\mathcal{R}$, $L_2 = -\mathcal{R}/2$. Hence, we find

$$F = 1 - 2\frac{\langle\langle\widetilde{0}|\mathcal{R}\mathcal{G}\mathcal{R}|0\rangle\rangle}{\langle\langle\widetilde{0}|\mathcal{R}|0\rangle\rangle}. \tag{5.22}$$

This is a central expression for the consequent sections. Yet, in order to employ (5.22) we need to know the explicit structure of the matrix $\mathcal{G}$. To determine it, we construct the orthogonal complement to the vectors $|0\rangle\rangle$ and $\langle\langle\widetilde{0}|$. By that we mean two sets of $2S$ linearly independent vectors, $|\alpha\rangle\rangle$ and $\langle\langle\widetilde{\alpha}|$ which satisfy

$$\langle\langle\widetilde{\alpha}|0\rangle\rangle = \langle\langle\widetilde{0}|\alpha\rangle\rangle = 0, \qquad \alpha = 1, 2, ...2S. \tag{5.23}$$

Projecting equation (5.17) onto states $\langle\langle\widetilde{\alpha}|$ and $|\beta\rangle\rangle$ we obtain

$$G_{\alpha\gamma}\mathfrak{g}^{-1}_{\gamma\delta}L^0_{\delta\beta} = \mathfrak{g}_{\alpha\beta}. \tag{5.24}$$

Here $\mathfrak{g}_{\alpha\beta} = \langle\langle\widetilde{\alpha}|\beta\rangle\rangle$ is a Gramian matrix for the described vector sets. To derive equation (5.24) we resolved unity as

$$\hat{1} = |0\rangle\rangle\langle\langle\widetilde{0}| + \sum_{\alpha,\beta=1}^{2S} |\widetilde{\alpha}\rangle\rangle\mathfrak{g}^{-1}_{\alpha\beta}\langle\langle\beta|. \tag{5.25}$$

In contrast to the full evolution operator, the $2S \times 2S$ matrix $L^0_{\delta\beta}$ is invertible. Hence, we find

$$G_{\alpha\beta} = \mathfrak{g}_{\alpha\delta}\left(L^0\right)^{-1}_{\delta\gamma}\mathfrak{g}_{\gamma\beta}. \tag{5.26}$$

Substitution of two unity resolutions (5.25) into equation (5.22) yields

$$F = 1 - 2\frac{\langle\langle\widetilde{0}|\mathcal{R}|\alpha\rangle\rangle\left(L^0\right)^{-1}_{\alpha\beta}\langle\langle\widetilde{\beta}|\mathcal{R}|0\rangle\rangle}{\langle\langle\widetilde{0}|\mathcal{R}|0\rangle\rangle}. \tag{5.27}$$

At this stage, we need to make a convenient choice of the orthogonal complements $\langle\langle\widetilde{\alpha}|$ and $|\alpha\rangle\rangle$

($\alpha = 1, 2, ..., 2S$). We found sets of vectors for which $L^0_{\alpha\beta}$ is diagonal. The left eigenvector corresponding to $\epsilon_1^{\lambda=0} = 0$ is $\langle\langle\widetilde{0}| = (1, 1, 1, ..., 1)$. The orthogonal complement to $\langle\langle\widetilde{0}|$ is given by

$$
\begin{aligned}
|1\rangle\rangle &= (1, 0, 0, ..., 0, 0)^T - \frac{1}{\mathcal{Z}}\left(\vartheta^S, \vartheta^{S-1}, \vartheta^{S-2}, ..., \vartheta^{-S}\right)^T, \\
|2\rangle\rangle &= (1, 1, 0, ..., 0, 0)^T - \frac{2}{\mathcal{Z}}\left(\vartheta^S, \vartheta^{S-1}, \vartheta^{S-2}, ..., \vartheta^{-S}\right)^T, \\
&... \\
|2S\rangle\rangle &= (1, 1, 1, ..., 1, 0)^T - \frac{2S}{\mathcal{Z}}\left(\vartheta^S, \vartheta^{S-1}, \vartheta^{S-2}, ..., \vartheta^{-S}\right)^T.
\end{aligned} \tag{5.28}
$$

Here, once again, $\mathcal{Z} = \sum_{m=-S}^{S} \vartheta^m$. The orthogonal complement of the right eigenvector $|0\rangle\rangle$ is

$$
\begin{aligned}
\langle\langle\widetilde{1}| &= \mathcal{Z}\left(\vartheta^{-S}, 0, 0, ..., 0, 0\right) - (1, 1, 1, ..., 1), \\
\langle\langle\widetilde{2}| &= \mathcal{Z}\left(\vartheta^{-S}, \vartheta^{-S+1}, 0, ..., 0, 0\right) - 2(1, 1, 1, ..., 1), \\
&... \\
\langle\langle\widetilde{2S}| &= \mathcal{Z}\left(\vartheta^{-S}, \vartheta^{-S+1}, \vartheta^{-S+2}, ..., \vartheta^{S-1}, 0\right) - 2S(1, 1, 1, ..., 1).
\end{aligned} \tag{5.29}
$$

Using expressions (5.28) and (5.29) for $L^0_{\alpha\beta} = \langle\langle\widetilde{\alpha}|L^0|\beta\rangle\rangle$ we find

$$
L^0_{\alpha\beta} = -\eta_- \frac{S(S+1) - (S-\alpha+1)(S-\alpha)}{4} \frac{\vartheta^{-S+\alpha-1}}{\mathcal{Z}} \delta_{\alpha\beta}, \qquad \alpha, \beta = 1, 2, ..., 2S, \tag{5.30}
$$

so that $L^0_{\alpha\beta}$ is indeed diagonal. Next, we obtain

$$
\begin{aligned}
\langle\langle\widetilde{0}|\mathcal{R}|\alpha\rangle\rangle = \eta_- \sum_{m=S-\alpha+1}^{S} \left\{\kappa m^2 + \frac{1}{4}(S(S+1) - m(m+1))\vartheta + \frac{1}{4}(S(S+1) - m(m-1))\right\} - \\
-\eta_- \frac{\alpha}{\mathcal{Z}} \sum_{m=-S}^{S} \left\{\kappa m^2 + \frac{1}{4}(S(S+1) - m(m+1))\vartheta + \frac{1}{4}(S(S+1) - m(m-1))\right\} \vartheta^m = \langle\langle\widetilde{\alpha}|\mathcal{R}|0\rangle\rangle
\end{aligned} \tag{5.31}
$$

and, finally,

$$
\langle\langle\widetilde{0}|\mathcal{R}|0\rangle\rangle = \frac{\eta_-}{\mathcal{Z}} \sum_{m=-S}^{S} \left\{\kappa m^2 + \frac{1}{4}(S(S+1) - m(m+1))\vartheta + \frac{1}{4}(S(S+1) - m(m-1))\right\} \vartheta^m. \tag{5.32}
$$

Note that according to equations (5.27), (5.30), (5.31), and (5.32), the Fano factor is always larger than unity. Moreover, we expressed the Fano factor through ϑ and κ only. In turn, this implies that the Fano factor is a function of C and B only for any S.

The discussed equations deliver a straightforward method for the evaluation of Fano factor for any given impurity spin S: all of the aforementioned sums except one can be easily evaluated. Therefore, in principle we can write down the expression for the Fano factor that has a single summation. While the obtained result is in general rather bulky and not very practical, it allows for an elegant description of the case $B \ll 1$, in which the stationary state density matrix of the magnetic impurity is proportional to the identity matrix.

5.4.1 Fano factor for a non-polarized magnetic impurity

In the limit $B \ll 1$ the Gibbs factor is close to unity, $\vartheta = (1+\sqrt{B})(1-\sqrt{B}) \approx 1$, and the steady state density matrix is approximately

$$|0\rangle\rangle = \frac{1}{2S+1}(1,1,1,...,1)^T. \tag{5.33}$$

Therefore, the magnetic impurity occupies all of its $2S+1$ states with equal probability. In that case it is possible to analytically perform of the summations in equations (5.27), (5.30), (5.31), and (5.32). We find

$$\langle\langle\widetilde{0}|\mathcal{R}|0\rangle\rangle = \eta_- \frac{1}{3} S(S+1)(2S+1)^2(1+\kappa),$$

$$\langle\langle\widetilde{0}|\mathcal{R}|\alpha\rangle\rangle = \eta_- \frac{2S+1}{12}\alpha(2S+1-\alpha)(2S+1-2\alpha)(1-2\kappa). \tag{5.34}$$

As a result, we conclude

$$F = 1 + \frac{(2S-1)(2S+3)}{45}\frac{(1-2\kappa)^2}{1+\kappa} = 1 + \frac{(2S-1)(2S+3)}{45}\frac{(3C-2)^2}{C}. \tag{5.35}$$

This expression is remarkable for several reasons:

- For $S = 1/2$ the Fano factor of the backscattering current is unity in the considered limit.
- The Fano factor for $B \ll 1$ might be larger than 2, in the contrast to the case $S = 1/2$. If we consider $C = 1$, we find that $F < 2$ for the magnetic impurity with $S < 3$, $F = 2$ for the impurity with $S = 3$, and $F > 2$ for $S > 3$.
- $F = 1$ for $C = 2/3$. For any fixed $C \neq 2/3$ the Fano factor scales as S^2 in the limit $S \gg 1$.
- The Fano factor diverges at $C = 0$. This peculiarity might seem surprising at first, but we will demonstrate that it is common for any $0 \leq B < 1$. Physical reasoning for this divergence will be also provided later.

5.5 Fano factor for a polarized magnetic impurity

In this section we consider the limit $1 - B \ll 1$. This regime corresponds to the large Gibbs factor $\vartheta \simeq 4/(1 - B) \gg 1$, i.e. to the almost fully polarized state of the magnetic impurity.

In terms of the magnetic impurity dynamics, the impurity spin almost always stays in the state with $S_z = S$ and rarely jumps to the $S_z = S - 1$ state. Therefore, in the leading non-trivial approximation only two levels with the largest occupations may be considered for the evaluation of the Fano factor. Projecting the generalized master equation (5.7) onto the subspace $S_z = S, S-1$ we see that to required order in λ the generating function of the backscattering current is given by the solution of the secular equation

$$\det \begin{pmatrix} S^2\left(e^{-i\lambda}-1\right)\eta_{zz} - S\eta_-/2 - \epsilon^\lambda & S\eta_+ e^{-i\lambda}/2 \\ S\eta_- e^{-i\lambda}/2 & (S-1)^2\left(e^{-i\lambda}-1\right)\eta_{zz} - S\eta_+/2 - \epsilon^\lambda \end{pmatrix} = 0 \quad (5.36)$$

with the largest real part. We use this expression to analyze various limiting cases. First, we assume that $1 - C \gg 1 - B$. Then we find

$$F = 1 + \frac{1-B}{1-C}\frac{(2S - 1 - C(3S-1))^2}{2CS^3}. \quad (5.37)$$

The Fano factor at $B = 1$ is strictly unity. At finite fixed $1 - B$ expression (5.37) contains divergence at small C, just as it was in the case $B \ll 1$ (see (5.35) for details). Note that if we fix the ratio of small C and small $1 - B$ constant and then reduce C, the Fano factor saturates at a finite value. Let us assume $C = \rho\cos\phi$, $1 - B = \rho\sin\phi$, and $\rho \to 0$. Then

$$F = 1 + \tan\phi\frac{(2S-1)^2}{2S^3}. \quad (5.38)$$

For $S > 1/2$ the Fano factor changes from 1 to ∞ as ϕ is changed from 0 to $\pi/2$. It is important to underline that for $S \gg 1$ the difference $F - 1$ goes to zero as $1/S$.

As a next step, we consider the exceptional point $B = C = 1$ with $\langle\langle \Delta N^n \rangle\rangle = 0$. Near this point the Fano factor also depends explicitly on the direction in which we approach the exceptional point. Once again, we fix some direction ϕ: $1 - C = \rho\cos\phi$, $1 - B = \rho\sin\phi$ and then reduce ρ to zero. In that case, the limiting expression for the Fano factor is

$$F = 2 - \frac{2S}{\tan\phi + 2S}. \quad (5.39)$$

Notice, that in the this regime the Fano factor changes from 1 to 2 smoothly as ϕ changes from 0

($B = 1$) to $\pi/2$ ($C = 1$). For $S = 1/2$ equation (5.39) coincides with equation (5.6). In the next subsection we show that for $C = 1$ the Fano factor may exceed 2 in the regime $1 - B \ll 1$. To capture that it is necessary to take into account transitions between three levels with the highest occupation probabilities.

5.5.1 Three-level regime

In a three-level model for the case $C = 1$ the generating function of the backscattering current is given as solution of the secular equation

$$\det \begin{pmatrix} -\eta_- \frac{S}{2} - \epsilon^\lambda & \eta_+ \frac{S}{2} e^{-i\lambda} & 0 \\ \eta_- \frac{S}{2} e^{-i\lambda} & -\eta_+ \frac{S}{2} - \eta_- \frac{2S-1}{2} - \epsilon^\lambda & \eta_+ \frac{2S-1}{2} e^{-i\lambda} \\ 0 & \eta_- \frac{2S-1}{2} e^{-i\lambda} & -\eta_+ \frac{2S-1}{2} - \epsilon^\lambda \end{pmatrix} = 0 \tag{5.40}$$

with the largest real part. To the first order in $1 - B$ we find

$$F \simeq 2 + \frac{S-1}{S}(1 - B). \tag{5.41}$$

Therefore, for the magnetic impurity with spin $S > 1$ the correction to $F = 2$ of the first order in $1 - B$ is positive. At the same time, for $S = 1$ it nullifies and for $S = 1/2$ it is negative which is consistent with equation (5.4) that limits the Fano factor to the interval $1 \leq F \leq 2$. Note that our three-level scheme gives the correct result for the spin-1/2 (two-level) case.

5.6 Qualitative discussion

5.6.1 Polarized impurity

First of all, for $B = 1$ we find $F = 1$. This result is expected and physically justified because $B = 1$ corresponds to the classical magnetic impurity that always stays in the state $S_z = S$. Therefore, the only allowed backscattering processes happen due to $\mathcal{J}_{zx}$ and $\mathcal{J}_{zy}$ terms in the impurity-electron coupling. These terms are responsible for the scattering of helical edge electrons not accompanied with impurity spin-flips. This means that the impurity does not keep memory about backscattered electrons leading to Poisson single-electron reflection process with $F = 1$. Realistic graph of the backscattering current as a function of time is shown in Figure 5.2.

For finite but small difference $1 - B$ rare correlated two-particle reflections enter the picture described above. These two-particle processes happen because at some moments of time the im-

purity spin flips to the state $S_z = S - 1$, lives there for a very short time, and then flips back. Each flipping leads to a single backscattered electron resulting in an overall two-particle scattering. This results in $F - 1 \propto 1 - B$. The backscattering current as a function of time is plotted in Figure 5.3. For $S = 1/2$ and $1 - B \ll 1$ we have shown explicitly that the backscattering is a superposition of independent Poisson single-particle and two-particle processes (see equation (4.43) for details).

5.6.2 Exceptional point

Although for $1 - B \ll 1$ and for generic $C \lesssim 1$ the physical picture described above is valid, some care is needed near the point $B = C = 1$. This point corresponds to the absence of the backscattering current because $B = C = 1$ implies $\mathcal{J}_{zx} = \mathcal{J}_{zy} = \mathcal{J}_{yx} = 0$ and $\mathcal{J}_{xx} = \mathcal{J}_{yy}$. For this reason, the value of the Fano factor becomes sensitive to the direction at which we approach the exceptional point, as indicated by formula (5.39). For $B = 1$, $C \to 1$ Fano factor is exactly unity because the only backscattering is due to $\mathcal{J}_{zx}$ and $\mathcal{J}_{zy}$. For $C = 1$, $B \to 1$ Fano factor is close to two as $\mathcal{J}_{zx} = \mathcal{J}_{zy} = 0$ and the only backscattering happens in pairs due to the double-flip mechanism (see Figure 5.4).

5.6.3 Divergence of the Fano factor

As it was shown, the Fano factor for the impurity with a large spin diverges as $1/C$ at small C if $1 - B \ll 1$ (see equation (5.37)) and if $B \ll 1$ (see Eq. (5.35)). We find that for $S > 1/2$ this behavior is generic, i.e. the divergence at small C happens for any fixed B. This can be easily seen from equation (5.27). Indeed, when $C \to 0$, parameter κ becomes large and $\mathcal{R}$ operator can be estimated as $\mathcal{R} \propto \kappa\eta_-$. At the same time, $\mathcal{G} \propto 1/\eta_-$. Therefore, the resulting expression scales as $F \propto \eta_-\kappa \propto 1/C$. Note that for $S = 1/2$ the additional cancellation happens and the Fano factor remains finite at small C in accordance with (5.4).

Now we physically interpret the divergence at small C for $S > 1/2$. For the sake of simplicity,

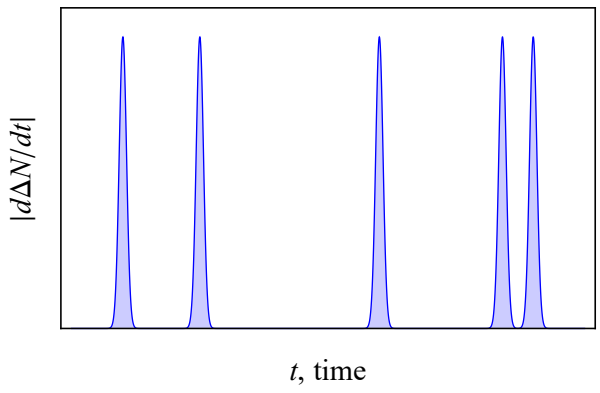

Figure 5.2: Sketch of the backscattering current as a function of time in the case $B = 1$. Backscattering is a single-particle Poisson process.

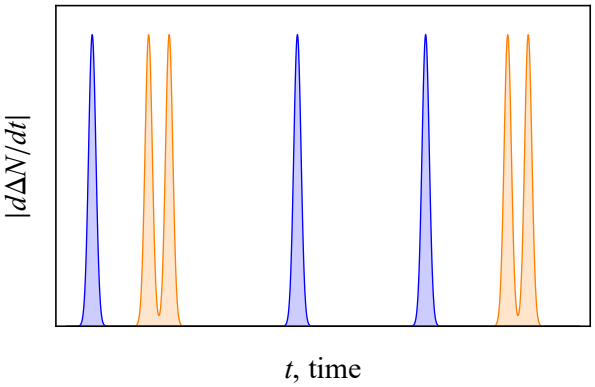

Figure 5.3: Sketch of the backscattering current as a function of time in the case $B \approx 1$. Rare pairwise reflections (orange) appear.

let us initially assume that $S = 1$. Then, according to the definition of C, coupling constants $\mathcal{J}_{zx}$ and $\mathcal{J}_{zy}$ are very large in comparison to $\mathcal{J}_{xx}$, $\mathcal{J}_{yy}$, and $\mathcal{J}_{yx}$ provided C is small. Therefore, the reflection happens mainly due to processes which do not require impurity flips. However, according to the Fermi Golden rule, the intensity of such processes is proportional to S_z^2, because they enter the Hamiltonian either as $\mathcal{J}_{zx}S_z s_x$ or $\mathcal{J}_{zy}S_z s_y$. This makes the backscattering current very sensitive to the spin projection of the impurity: for $S_z = 1$ the backscattering is frequent, while for $S_z = 0$ it is suppressed. Then, despite processes associated with $\mathcal{J}_{xx}$, $\mathcal{J}_{yy}$, and $\mathcal{J}_{yx}$ terms in the Hamiltonian are incapable of producing significant backscattering current, they can move the impurity from one state to another switching efficient backscattering on and off. For this reason, the backscattering current as a function of time looks like a series of long pulses, each containing a large number of backscattered electrons (sketched in Figure 5.5). The smaller C is the larger is the number of electrons in each pulse. Therefore, Fano factor diverges as parameter C is reduced towards zero.

For spin not equal to unity (e.g. $S = 3/2$) the pulses look differently because the intensity might drop less radically between the pulses (not to zero). Still, many-electron correlations are present and the Fano factor gets large at small C. Interestingly, if we consider some fixed B so that $1 - B \ll 1$ and small C, the Fano factor reduces as spin is increased as indicated by equation (5.37). That is because in the considered case only states with $S_z = S$ and $S_z = S - 1$ are relevant.

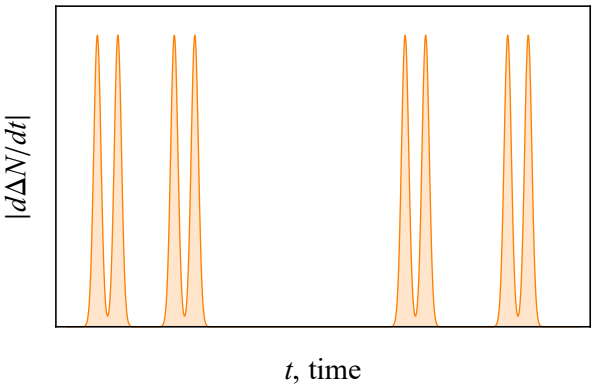

Figure 5.4: Sketch of the backscattering current as a function of time in the case $C = 1$, $1 - B \ll 1$. Backscattering is a two-particle Poisson process.

Therefore, the relative drop of the intensity of the backscattering current between the pulses is $\propto (1-1/S)^2 \to 1$ as $S \to +\infty$. This means that the correlations are smeared for $S \gg 1$.

5.6.4 Non-polarized magnetic impurity

In this subsection, we discuss the behavior of the system when $B \to 0$. Small B implies that the Gibbs factor $\vartheta \approx 1$ so that the impurity occupies all its levels with approximately the same probability. Formula (5.35) demonstrates that for large S the Fano factor scales as S^2. This can be easily explained. First of all, we note that temporal dynamics of the impurity is diffusive. Therefore, if the magnetic impurity starts its motion in some state $|S_z\rangle$, on average $\sim S^2$ hops happen before the spin projection returns to its initial value. Therefore, around S^2 of subsequent magnetic impurity flips are correlated. These correlations in the dynamics of the impurity are mimicked by correlations in the electron backscattering and S^2 scaling is reproduced in the Fano factor.

5.6.5 Qualitative description of the intermediate cases

If $C = 1$, then each impurity flip leads to a single backscattering event. As B is increased the system comes from the diffusive scattering regime to the regime in which electrons are backscattered in pairs. The Fano factor approaches 2 from below for $S = 1/2$ and from above for $S \geq 3/2$ as it was shown in (5.41). Interestingly, together with (5.35) this means that the Fano factor changes in a non-monotonous fashion along the line $C = 1$ at least for $S = 3/2, 2, 5/2, 3$.

If both C and B are just some numbers, then typically the Fano factor is close to unity for $S \gg 1$. Interestingly, F seems to be especially close to unity at the line $C = 2/3$. For example, the trace of this fact can be seen in (5.35). Moreover, at any given B so that $1 - B \ll 1$ the difference $F - 1$ is minimal at $C = (2S-1)/(3S-1) \approx 2/3$ as indicated by (5.37). Overall, the dependence of the Fano factor on B and C is summarized in Figure 5.6.

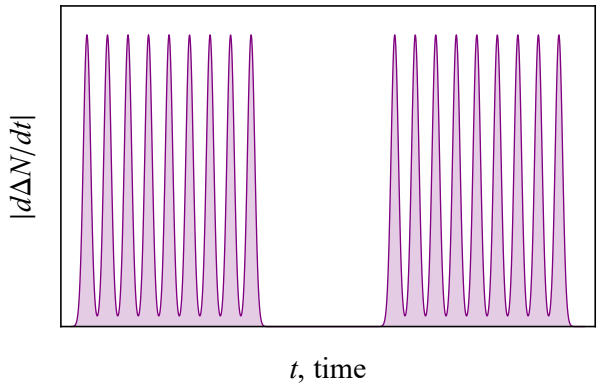

Figure 5.5: Sketch of the backscattering current as a function of time in the case $C \ll 1$, $S = 1$. Backscattering happens in long pulses.

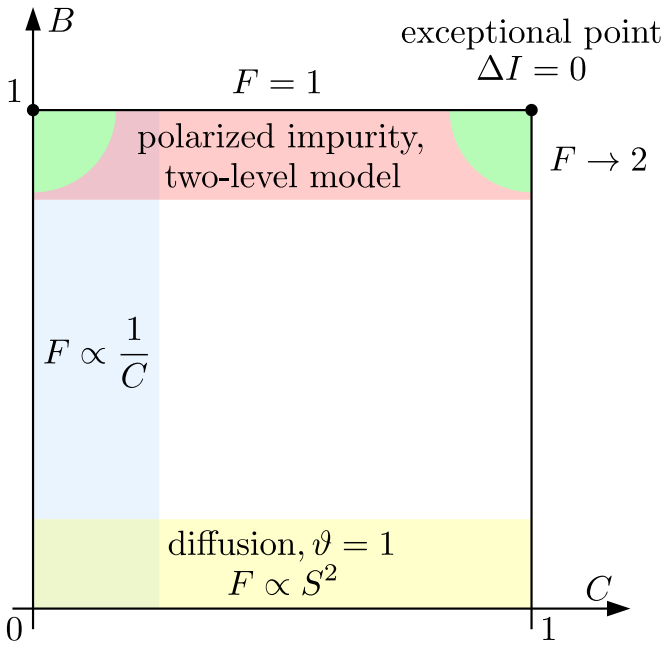

Figure 5.6: Different regimes for $S > 1/2$. For $B \ll 1$ (yellow) the impurity occupies all energy levels with the same probability, $F \propto S^2$ for large S. For $1 - B \ll 1$ (red) the impurity is almost fully polarized and only two levels are relevant, $F - 1 \propto 1 - B$. For $C \ll 1$ (blue) backscattering happens in long pulses and $F \propto 1/C$. In the vicinity of the point $(1, 1)$ (green) F changes from 1 to 2 depending on the direction. In the vicinity of $(0, 1)$ (green) the Fano factor changes from 1 to ∞ depending on the direction.

Features, indicated in Figure 5.6 and described above, can be identified in Figure 5.7 which presents the exact map of the Fano factor for the spin-1 impurity. It can be seen that the Fano factor strongly depends on the direction of approach for points $B = 1, C = 0$ and $B = 1, C = 1$. Moreover, the Fano factor for $B < 1$ diverges at $C \ll 1$ as $F \propto 1/C$.

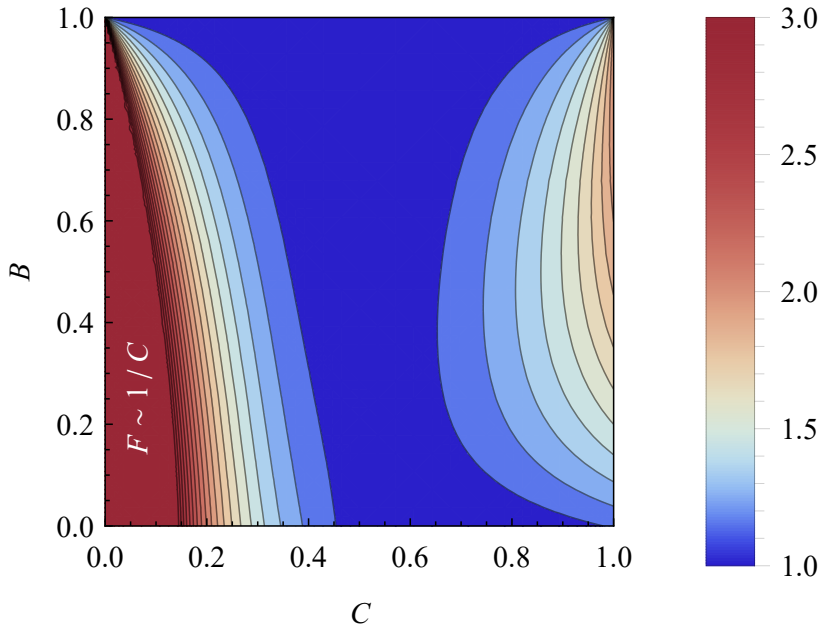

Figure 5.7: F for different B and C in the case $S = 1$. The divergence $F \sim 1/C$ for $C \ll 1$ is a general feature of $S > 1/2$. Near $C = B = 1$ Fano factor changes from 1 to 2.

Chapter 6

Conclusion

In the present thesis we considered the electrical current flowing along the edge of a two-dimensional topological insulator. We assumed that a single magnetic impurity with spin S is located near the edge. The goal of the work was to investigate the statistics of backscattering current ΔI induced by the impurity when finite voltage V is applied to the edge. Main results of the thesis are the following:

- We derived the generalized master equation for the density matrix of the magnetic impurity (3.33). This equation can be used to calculate the cumulant generating function of the backscattering current.
- We studied the stationary state of the magnetic impurity. For $V \gg \mathcal{J}T$ its the steady state density matrix is given by (4.19).
- We obtained the general expression (4.3) that links the backscattering current to impurity spin averages $\langle S_i \rangle$ and $\langle S_i S_j \rangle$ calculated in the steady state.
- Using (4.3) we evaluated the average backscattering current for arbitrary S for $V \ll T$. The result is given by the equation (4.9). The backscattering conductance ΔG has a crossover at $V \sim \mathcal{J}T$. For $S = 1/2$ the backscattering conductance saturates just after the crossover at $V \sim \mathcal{J}T$. For $S > 1/2$ the backscattering conductance saturates at $V \sim T$.
- For $S = 1/2$ we obtained expression (4.34) for the zero-frequency noise of the backscattering current that is valid at arbitrary voltage.
- In the case $S = 1/2$ and $V \gg \mathcal{J}T$ we derived the full cumulant generating function (4.42). We found that for certain parameters of the system.

- We realized that for any S the Fano factor of the backscattering current can be expressed as a function of two dimensionless parameters of the electron-impurity coupling matrix. The first parameter is called B, it satisfies $0 \leq B \leq 1$ and is given by (4.22). The second parameter C is also from zero to unity, it is given by (4.36).

- We calculated the Fano factor for $1 - B \ll 1$ - see equation (5.37). Moreover, we derived the expression for the Fano factor in the limit $B \ll 1$ - see equation (5.35).

- Finally, we discussed the behavior of the Fano factor for arbitrary S, C and B.

In the future research, we will try to understand how electron-electron interactions alter the picture of the helical edge transport described above.

Bibliography

[1] X.-L. Qi and S.-C. Zhang. Topological insulators and superconductors. *Rev. Mod. Phys.*, 83:1057, 2011.

[2] M. Z. Hasan and C. L. Kane. *Colloquium*: Topological insulators. *Rev. Mod. Phys.*, 82:3045, 2010.

[3] L. Fu and C. L. Kane. Topological insulators with inversion symmetry. *Phys. Rev. B*, 76:045302, 2007.

[4] D. Hsieh, D. Qian, L. Wray, Y. Xia, Y. S. Hor, R. J. Cava, and M. Z. Hasan. A topological Dirac insulator in a quantum spin Hall phase. *Nature*, 452(7190):970, 2008.

[5] Y. Ando. Topological insulator materials. *Journal of the Physical Society of Japan*, 82(10):102001, 2013.

[6] T. Sato, K. Segawa, H. Guo, K. Sugawara, S. Souma, T. Takahashi, and Y. Ando. Direct evidence for the dirac-cone topological surface states in the ternary chalcogenide $TlBiSe_2$. *Phys. Rev. Lett.*, 105:136802, 2010.

[7] C. L. Kane and E. J. Mele. $\mathbb{Z}_2$ topological order and the quantum spin Hall effect. *Phys. Rev. Lett.*, 95:146802, 2005.

[8] C. L. Kane and E. J. Mele. Quantum spin Hall effect in graphene. *Phys. Rev. Lett.*, 95:226801, 2005.

[9] B. A. Bernevig, T. L. Hughes, and S.-C. Zhang. Quantum spin Hall effect and topological phase transition in HgTe quantum wells. *Science*, 314(5806):1757, 2006.

[10] M. König, S. Wiedmann, C. Brüne, A. Roth, H. Buhmann, L. W. Molenkamp, X.-L. Qi, and S.-C. Zhang. Quantum spin Hall insulator state in HgTe quantum wells. *Science*, 318(5851):766, 2007.

[11] A. Roth, C. Brüne, H. Buhmann, L. W. Molenkamp, J. Maciejko, X.-L. Qi, and S.-C. Zhang. Nonlocal transport in the quantum spin Hall state. *Science*, 325(5938):294–297, 2009.

[12] G. M. Gusev, Z. D. Kvon, O. A. Shegai, N. N. Mikhailov, S. A. Dvoretsky, and J. C. Portal. Transport in disordered two-dimensional topological insulators. *Phys. Rev. B*, 84:121302, 2011.

[13] C. Brüne, A. Roth, H. Buhmann, E. M. Hankiewicz, L. W. Molenkamp, J. Maciejko, X.-L. Qi, and S.-C. Zhang. Spin polarization of the quantum spin Hall edge states. *Nature Physics*, 8(6):485, 2012.

[14] K. C. Nowack, E. M. Spanton, M. Baenninger, M. König, J. R. Kirtley, B. Kalisky, C. Ames, P. Leubner, C. Brüne, H. Buhmann, et al. Imaging currents in HgTe quantum wells in the quantum spin Hall regime. *Nature materials*, 12(9):787, 2013.

[15] G. M. Gusev, Z. D. Kvon, E. B. Olshanetsky, A. D. Levin, Y. Krupko, J. C. Portal, N. N. Mikhailov, and S. A. Dvoretsky. Temperature dependence of the resistance of a two-dimensional topological insulator in a HgTe quantum well. *Phys. Rev. B*, 89:125305, 2014.

[16] A. Kononov, S. V. Egorov, Z. D. Kvon, N. N. Mikhailov, S. A. Dvoretsky, and E. V. Deviatov. Evidence on the macroscopic length scale spin coherence for the edge currents in a narrow HgTe quantum well. *JETP Letters*, 101(12):814–819, 2015.

[17] J. I. Väyrynen, M. Goldstein, and L. I. Glazman. Helical edge resistance introduced by charge puddles. *Phys. Rev. Lett.*, 110:216402, 2013.

[18] J. I. Väyrynen, M. Goldstein, Y. Gefen, and L. I. Glazman. Resistance of helical edges formed in a semiconductor heterostructure. *Phys. Rev. B*, 90:115309, 2014.

[19] L. Kimme, B. Rosenow, and A. Brataas. Backscattering in helical edge states from a magnetic impurity and rashba disorder. *Phys. Rev. B*, 93:081301, 2016.

[20] P. D. Kurilovich, V. D. Kurilovich, I. S. Burmistrov, and M. Goldstein. Helical edge transport in the presence of a magnetic impurity. *JETP Letters*, 106(9):593–599, 2017.

[21] R. A. Niyazov, D. N. Aristov, and V. Yu. Kachorovskii. Tunneling Aharonov-Bohm interferometer on helical edge states. *arXiv:1804.01115*, 2018.

[22] C. Xu and J. E. Moore. Stability of the quantum spin Hall effect: Effects of interactions, disorder, and $\mathbb{Z}_2$ topology. *Phys. Rev. B*, 73:045322, 2006.

[23] J. Wang, Y. Meir, and Y. Gefen. Spontaneous breakdown of topological protection in two dimensions. *Phys. Rev. Lett.*, 118:046801, 2017.

[24] J. Maciejko. Kondo lattice on the edge of a two-dimensional topological insulator. *Phys. Rev. B*, 85:245108, 2012.

[25] B. L. Altshuler, I. L. Aleiner, and V. I. Yudson. Localization at the edge of a 2D topological insulator by Kondo impurities with random anisotropies. *Phys. Rev. Lett.*, 111:086401, 2013.

[26] O. M. Yevtushenko, A. Wugalter, V. I. Yudson, and B. L. Altshuler. Transport in helical luttinger liquid with Kondo impurities. *EPL (Europhysics Letters)*, 112:57003, 2015.

[27] J. I. Väyrynen, F. Geissler, and L. I. Glazman. Magnetic moments in a helical edge can make weak correlations seem strong. *Phys. Rev. B*, 93:241301, 2016.

[28] O. M. Yevtushenko and V. I. Yudson. Kondo impurities coupled to a helical luttinger liquid: RKKY-Kondo physics revisited. *Phys. Rev. Lett.*, 120:147201, 2018.

[29] J. I. Väyrynen and L. I. Glazman. Current noise from a magnetic moment in a helical edge. *Phys. Rev. Lett.*, 118:106802, 2017.

[30] D. G. Rothe, R. W. Reinthaler, C.-X. Liu, L. W. Molenkamp, S.-C. Zhang, and E. M. Hankiewicz. Fingerprint of different spin–orbit terms for spin transport in HgTe quantum wells. *New J. Phys.*, 12:065012, 2010.

[31] Otten D. Magnetic impurity coupled to helical edge states, 2013. Bachelor's thesis, Institute for Quantum Information, RWTH Aachen University.

[32] P. D. Kurilovich, V. D. Kurilovich, and I. S. Burmistrov. Indirect exchange interaction between magnetic impurities in the two-dimensional topological insulator based on CdTe/HgTe/CdTe quantum wells. *Phys. Rev. B*, 94:155408, 2016.

[33] S. A. Tarasenko, M. V. Durnev, M. O. Nestoklon, E. L. Ivchenko, J.-W. Luo, and A. Zunger. Split Dirac cones in HgTe/CdTe quantum wells due to symmetry-enforced level anticrossing at interfaces. *Phys. Rev. B*, 91:081302, 2015.

[34] M. V. Durnev and S. A. Tarasenko. Magnetic field effects on edge and bulk states in topological insulators based on HgTe/CdHgTe quantum wells with strong natural interface inversion asymmetry. *Phys. Rev. B*, 93:075434, 2016.

[35] G. M. Minkov, A. V. Germanenko, O. E. Rut, A. A. Sherstobitov, M. O. Nestoklon, S. A. Dvoretski, and N. N. Mikhailov. Spin-orbit splitting of valence and conduction bands in HgTe quantum wells near the Dirac point. *Phys. Rev. B*, 93:155304, 2016.

[36] M. Esposito, U. Harbola, and S. Mukamel. Nonequilibrium fluctuations, fluctuation theorems, and counting statistics in quantum systems. *Rev. Mod. Phys.*, 81:1665–1702, 2009.

[37] Á. Rivas and S.F. Huelga. *Open Quantum Systems: An Introduction*. SpringerBriefs in Physics. Springer Berlin Heidelberg, 2011.

[38] V. D. Kurilovich. Helical edge transport in the presence of a magnetic impurity, 2018. Master's thesis, Skolkovo Institute of Science and Technology.

[39] R. Žitko, R. Peters, and Th. Pruschke. Properties of anisotropic magnetic impurities on surfaces. *Phys. Rev. B*, 78:224404, 2008.